chemosensors

Review

Single-Entity Electrochemistry for Analytical Chemistry: Moving Towards the Limits of Detecting Single Molecules and Single Cells

Li Fu [1,*], Fei Chen [1], Yanfei Lv [1], Shichao Zhao [1] and Cheng-Te Lin [2,3,4]

[1] College of Materials and Environmental Engineering, Hangzhou Dianzi University, Hangzhou 310018, China
[2] Qianwan Institute, Ningbo Institute of Materials Technology and Engineering (NIMTE), Chinese Academy of Sciences, Ningbo 315201, China
[3] Center of Materials Science and Optoelectronics Engineering, University of Chinese Academy of Sciences, Beijing 100049, China
[4] Key Laboratory of Advanced Marine Materials, Ningbo Institute of Materials Technology and Engineering (NIMTE), Chinese Academy of Sciences, Ningbo 315201, China
* Correspondence: fuli@hdu.edu.cn

Abstract

Single-entity electrochemistry (SEE) expands the scope of analytical electrochemical measurement by shifting attention from ensemble-averaged currents to individually resolved stochastic events. This review evaluates progress toward two analytical endpoints, trustworthy detection of single molecules and context-preserving interrogation of single cells, with emphasis on quantitative rigor rather than platform novelty alone. Across nanoparticle collisions, nanopores, confined nanoelectrodes, vesicle electrochemical cytometry, intracellular nanopipettes, and array-enabled single-cell devices, the decisive analytical issue is no longer simply whether one entity can be detected, but whether event assignment, calibration, throughput, and reproducibility are sufficient to support credible inference. Representative primary studies are compared through shared metrics including event frequency, temporal resolution, bandwidth, molecular counts, detection limit, affinity, and effective yield of analyzable events. Particular attention is given to three recurring bottlenecks: interfacial variability, model-dependent event interpretation, and incomplete reporting of denominators such as rejected events, insertion success, and pore-to-pore or cell-to-cell reproducibility. The current evidence base is strongest in secretion and vesicle studies, whereas confinement-enabled and multimodal routes define the leading edge of single-molecule analysis. Overall, SEE is developing not as a single universal platform, but as a family of interface-controlled, data-rich analytical strategies whose future analytical value will depend on standardized reporting, multimodal validation, and benchmarking practices that preserve both sensitivity and confidence of assignment.

Keywords: single-entity electrochemistry; single-molecule detection; single-cell electrochemistry; nanopore sensing; nanoimpact electrochemistry; vesicle electrochemical cytometry

Check for updates

Received: 27 May 2026
Revised: 24 June 2026
Accepted: 29 June 2026
Published: 3 July 2026

Copyright: © 2026 by the authors. Licensee MDPI, Basel, Switzerland. This article is an open access article distributed under the terms and conditions of the Creative Commons Attribution (CC BY) license.

1. Introduction

Electroanalytical measurements are increasingly being judged not only by how sensitively an average signal can be measured, but also by whether an individual entity can be observed, assigned, and quantified before ensemble averaging erases functionally important heterogeneity. In electrochemistry, this shift is consequential because the readout

is interfacial, stochastic, and often fast. A catalytic nanoparticle colliding with an ultramicroelectrode, a single protein-modified carrier translocating through a nanopore, a vesicle releasing only a fraction of its content during exocytosis, or a single cell generating a localized impedance response can each produce transient electrical signals that are inaccessible in bulk measurements yet highly informative for analytical interpretation and biological context [1–4]. Single-entity electrochemistry (SEE) has therefore evolved from a specialized mechanistic area into a broader analytical framework for interrogating nanoparticles, molecules, vesicles, organelles, and cells one event at a time. The analytical significance of SEE extends beyond miniaturization. Distributions of individual events can be converted into information that bulk measurements would average away: collision frequencies reveal nanoparticle concentration and transport; blockade dwell times and amplitudes encode molecular size, charge, or binding state; amperometric spike integrals report vesicular content and release fractions; and multiplexed microelectrode arrays convert thousands of stochastic impacts into statistically meaningful descriptors of heterogeneity [2,5–7]. This perspective is important because the field is being pushed toward two limiting use cases. One is the detection of single molecules, where capture efficiency, noise, and false-positive assignment become limiting at the same scale as the signal itself. The other is the measurement of single cells, where electrochemical readouts must preserve viability, spatial context, and dynamic heterogeneity instead of simply maximizing sensitivity [8–10].

These two frontiers are related but not interchangeable. A platform that claims single-molecule sensitivity does not automatically deliver meaningful single-cell analytics, because the main bottleneck may shift from current noise to biological sampling, matrix effects, or the inability to assign a transient to a defined cellular process. Conversely, a platform that robustly resolves single-cell heterogeneity may still remain far from the molecular detection limit if background current, transport statistics, or interfacial fouling dominate the experiment. These four linked dimensions, the entity being probed, the interfacial architecture that localizes it, the stochastic signal it generates, and the analytical inference drawn from many such events, form the conceptual core of SEE (Figure 1). The field advances only when all four dimensions improve together rather than when one of them, usually nominal sensitivity, is optimized in isolation.

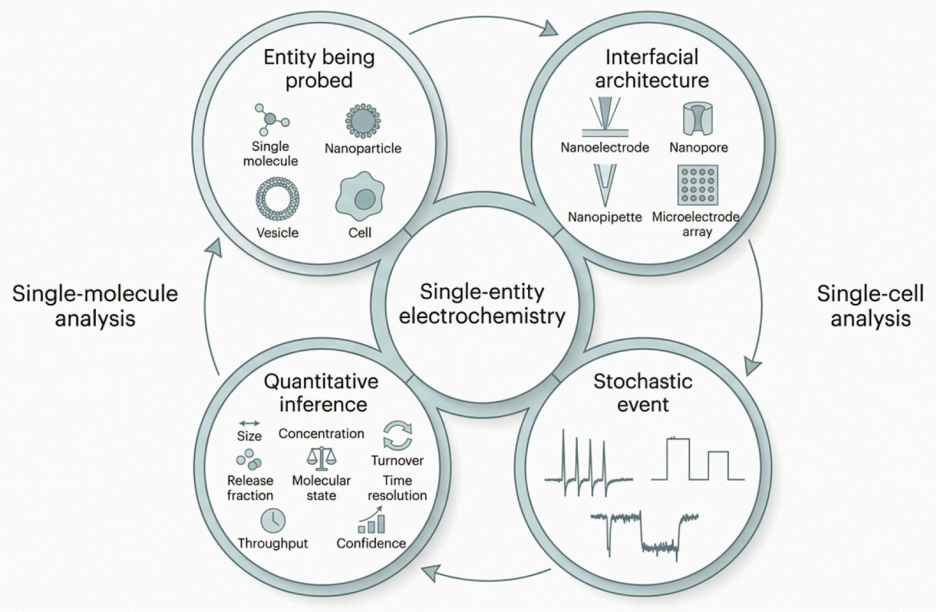


Figure 1. Concept-circle schematic summarizing how SEE connects electrochemical interfaces, stochastic events, quantitative metrics, and molecular or cellular targets.

This distinction justifies a more critical structure than the usual platform-by-platform survey. Recent primary studies have highlighted the breadth of SEE and its extension to electro-optical nanopores, high-throughput microelectrode arrays, impact-voltammetric kinetics, and high-content single-cell workflows [2,6,11,12]. The central analytical issue is not only what platforms exist, but how convincingly they move electrochemical analysis toward the practical limits of detecting one molecule or one cell. This assessment requires explicit comparison of signal levels, event confidence, time resolution, throughput, calibration logic, and susceptibility to false assignment. It also requires confronting the field's uneven maturity: some subareas now generate thousands of entity-resolved events in a few hours, whereas others still rely on low-throughput proof-of-concept experiments [6,13].

Accordingly, this review is organized around analytical limits rather than chronology. Section 2 defines what should count as a single entity in electroanalysis and compares the main transduction modes that have made SEE possible. Section 3 focuses on the route toward single-molecule electroanalysis, emphasizing both the promise of confinement-assisted and nanopore-enabled detection and the persistent gap between near-single-molecule claims and routine analytical deployment. Section 4 examines single-cell electrochemistry, from classic single-cell amperometry to newer intracellular and imaging-enabled formats. Section 5 then benchmarks the field across shared analytical metrics rather than technology labels, allowing direct comparison of sensitivity, temporal resolution, throughput, and assignment confidence. Finally, Section 6 identifies the technical and conceptual barriers that still separate compelling demonstrations from robust analytical workflows, before the Conclusion distills what SEE must achieve to become a mature analytical discipline.

2. Foundations and Enabling Toolbox of SEE

2.1. Defining the Single Entity in Electroanalysis

The phrase "single entity" encompasses several distinct epistemic claims. In the weakest sense, it means that individual transients are observed one at a time. In the stronger and analytically more useful sense, it means that a measured transient can be assigned to a physically defined entity and converted into a quantitative descriptor such as size, concentration, turnover, release fraction, and molecular state. Early discrete-event electrochemistry studies made this distinction concrete by showing that adsorption and collision events can be resolved individually rather than only as ensemble averages [1,14]. This definition excludes many superficially similar experiments in which single spikes are recorded but their origin remains ambiguous because adsorption, aggregation, interfacial restructuring, or instrumental artifacts cannot be ruled out.

Three criteria are therefore useful for deciding whether an experiment truly belongs to SEE. First, the experiment must isolate events in time, space, or both. Ultralow background currents at nanoelectrodes, confinement in nanopores or nanocavities, and sparse stochastic arrival statistics all serve this purpose [1,2,14]. Second, the event must be assignable to a bounded object or process. A catalytic current step can be informative if the particle collision model is constrained, but much less so if sticking, bouncing, and mediator depletion generate indistinguishable signatures. Third, the experiment must support a quantitative mapping between the event statistics and an analytical quantity, ideally with explicit treatment of capture efficiency, false-positive probability, and the number of events required for robust inference [5,6]. In practice, the field is strongest when all three criteria are satisfied and weakest when only the first one is.

This distinction matters because the main challenge of SEE is often not detection itself but confidence of assignment. A single-molecule platform may generate detectable current blockades while still failing analytically if one cannot separate specific from nonspecific

events. Likewise, a single-cell signal can be spatially localized without being biologically interpretable if it convolves secretion, transport, electrode fouling, and cell motion. The taxonomy shown in Figure 2 emphasizes that "single-entity" should therefore be treated as a layered claim: one layer concerns entity isolation, another concerns mechanistic assignment, and a third concerns quantitative readout. Only the combination of these layers moves the experiment toward genuine analytical utility.

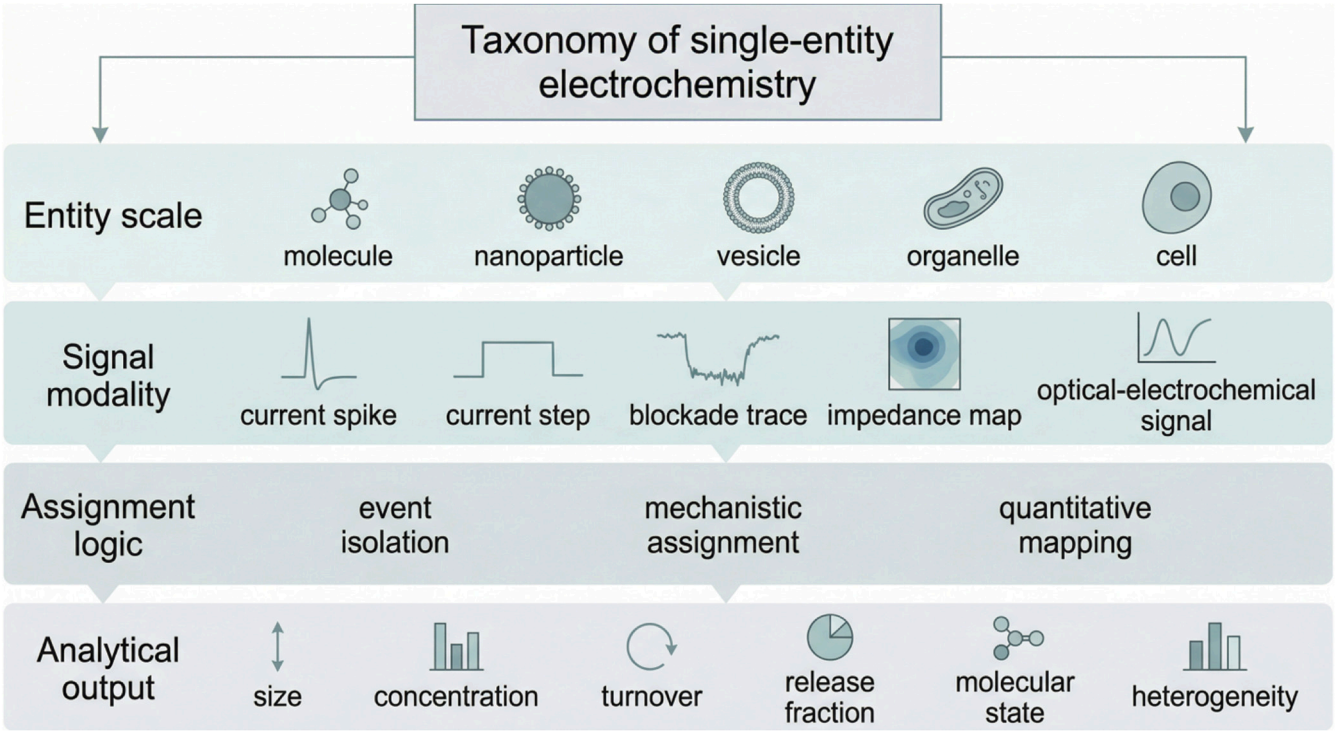


Figure 2. Taxonomy of SEE platforms across entity scale, signal modality, assignment logic, and analytical output.

2.2. Core Transduction Modes and Platform Architectures

The first major class of SEE platforms is collision or nanoimpact electrochemistry, in which suspended particles intermittently encounter an electrode and create current steps or spikes that report catalytic activity, blocking behavior, or particle size. This mode became foundational because it converted a formally random event, particle arrival at an electrode, into a statistically analyzable signal that could be repeated many times in a single experiment [1,15]. Recent studies continue to show why the approach remains attractive. Bai and co-workers used single-nanoparticle collision electrochemistry to follow thiol self-assembly on Au nanoparticles, illustrating how event-by-event transients can resolve nanoparticle surface chemistry that would be obscured in ensemble measurements [16]. Sundar and colleagues, in turn, showed how electrocatalytic amplification turns otherwise tiny particle encounters into larger, more analyzable signals, but also why that apparent gain in sensitivity can complicate calibration because signal magnitude reflects not only particle identity but mediator concentration, residence time, and landing geometry [17]. Read together, the two examples in Figure 3 show that the analytical attraction of nanoimpact electrochemistry and its central weakness arise from the same source: a simple event geometry can generate abundant transients, yet the inverse step from transient shape to unique particle property remains highly sensitive to interfacial chemistry and transport history.

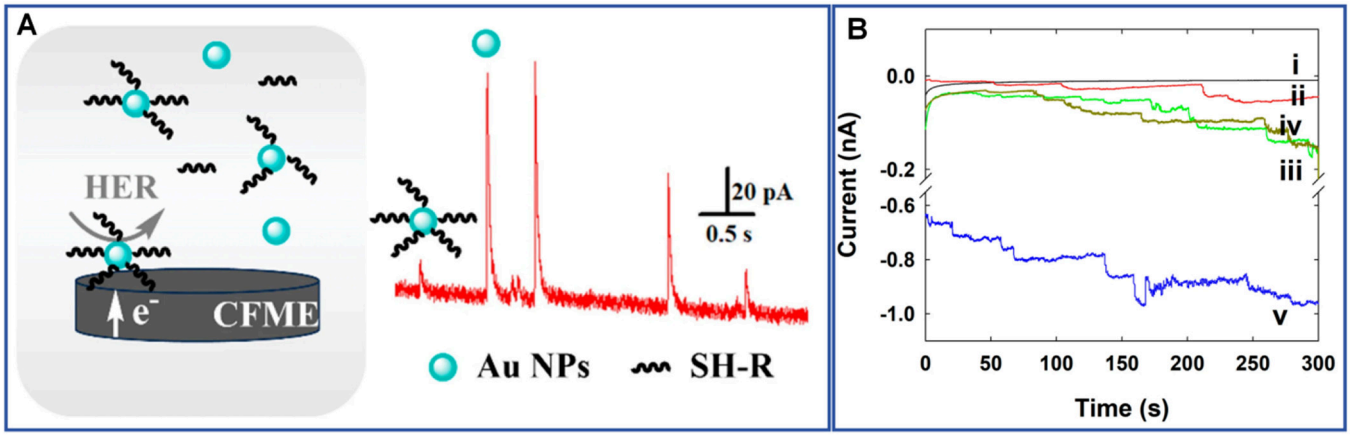


Figure 3. (**A**) Single-nanoparticle electrochemical collision-based method for monitoring the self-assembly processes of thiol molecules on the surface of Au NPs. (**B**) CA curves for single Au NPs collisions at the C-Fiber UME in pH 7.4 buffer solution (15 mM hydrazine) containing various concentrations of Au NPs (i) 0, (ii) 0.011, (iii) 0.023, (iv) 0.034, and (v) 0.045 pM at an applied potential of 0.25 V. Data acquisition time is 50 ms. Adapted from [16,17] under the terms of the Creative Commons Attribution License.

The maturation of collision electrochemistry is also visible in the way the field has diversified beyond simple event counting. SECM-guided collision studies showed that single-particle arrival frequencies can reproduce the expected negative-feedback dependence on tip-substrate spacing, meaning that stochastic impacts can recover ensemble transport physics when the geometry is well controlled [18]. Other work went further and used a single Pt nanoparticle collision to restore electron transfer through a tunneling ultramicroelectrode, effectively converting the entity itself into part of the sensing architecture [19]. More recent studies of single-particle oxygen-evolution catalysis and plasmon-enhanced nanoimpact electrochemistry then pushed the method toward heterogeneity mapping and coupled photoelectrochemistry [20,21]. These developments are analytically important because they show that collision electrochemistry is no longer only a way to detect that a particle arrived. It is becoming a route for measuring intrinsic catalytic diversity and even for constructing transient functional interfaces one entity at a time.

Another sign of maturity is that the field now treats transport and event encoding as design variables. Early work on current transients in single nanoparticle collisions already showed that steady-state impact currents and collision frequencies could be mapped onto particle size, concentration, and diffusion behavior instead of being dismissed as phenomenological spikes [22]. Surface chemistry quickly emerged as another control parameter: self-assembled monolayers on either the particle or the collector electrode modulated hydrazine-oxidation transients and therefore the apparent electrocatalytic signature of the same nominal nanoparticle [23]. Migration-driven collision experiments then showed that conductive nanoparticle impacts can deviate strongly from purely diffusive arrival statistics when the electric field and supporting electrolyte are operative parts of the experiment [24]. Tag-redox coulometry offered a non-destructive sizing route, recovering an average Ag nanoparticle radius of 45 ± 5 nm from particle–electrode collisions without consuming the particle during measurement [25]. At the catalytic end, methanol oxidation measured on nominal 50 nm Pt nanoparticles reached a maximum current density of 0.3 ± 0.2 mA cm^{-2} at +0.05 V, while sub-millisecond recording preserved transient heterogeneity [26]. Compositional tuning added another layer: Au-Pt nanoparticles favored a direct methanol-oxidation pathway around 0.6 V, whereas Pt alone emphasized the indirect CO-mediated route closer to 0.8 V, showing that single-particle SEE can resolve mechanistic pathway shifts as well as activity magnitude [27]. Even single redox enzymes

have entered this space: catalytic readout from HRP-modified nanoelectrodes produced staircase-like voltammetry and collision-style single-event signatures, underscoring that the border between single-particle and single-molecule electrochemistry is often set by interface architecture rather than analyte class alone [28].

An equally important broadening has been the rise of soft-entity SEE, where droplets, nanoemulsions, and transient nanoreactors become the entity under analysis. Single-droplet collisions turned emulsions into attoliter electrochemical reactors [29], while vitamin B_{12}-mediated dehalogenation on individual soft nanoparticles demonstrated that catalytic turnover can also be quantified one soft entity at a time [30]. Complete versus selective electrolysis of single emulsion droplets could be switched simply by changing the applied potential from −0.65 to −0.45 V [31]. Later studies pushed these systems beyond proof-of-concept detection: intact nanoemulsions were used to extract partition coefficients directly from single-entity events, reaching $P = 1.9\ (\pm 1.4) \times 10^{10}$ for 2-amino-6-bromobenzothiazole and revealing preconcentration by as much as eight orders of magnitude [32], while other work followed liquid–liquid interfacial kinetics in single nanodroplets [33], electrodeposited Au nanoparticles from droplets with radius of about 400 nm [34], and electrosynthesized Pd nanocatalysts from single-droplet reactors for downstream formic acid oxidation [35]. Practical deployment also improved when nanodroplet electrodeposition was redesigned so that the supporting salt resided in the aqueous phase, cutting operating cost by nearly three orders of magnitude without abandoning single-entity control [36]. Analytically, these studies extend SEE beyond detection of pre-existing objects: single entities can act as transient reactors, synthesis compartments, and interfacial metrology tools.

This soft-entity branch is especially valuable because it exposes event features that classical nanoparticle studies can miss. Femtoliter oil-droplet collisions were used to probe ion transfer across liquid–liquid interfaces directly at the single-droplet level [37], and inverse water-in-oil droplets extended that logic to a different emulsion topology instead of assuming that oil-in-water behavior is universal [38]. Surfactant-free nanodroplet reactors then showed that electrode potential can tune the size of Cu nanoparticles formed in individual droplets and that the same framework can be generalized to Ag and cobalt oxyhydroxide products [39]. One-step deposition of ligand-free PdPt alloy nanoparticles from water droplets added control over size, coverage, and elemental stoichiometry within the same droplet-mediated framework [40]. The nanoemulsion structure itself also became an analyte variable: monodisperse emulsions of about 40 nm diameter displayed composition-dependent event behavior [41], attoliter aqueous droplets could be detected even in electrolyte-free organic media [42], and collision–recollision trajectories revealed that some droplet signals encode post-impact dynamics rather than single-contact arrival [43]. Application-facing studies pushed further by using pluronic nanoemulsions to reach aromatic-toxicant detection limits down to 0.1 ppb [44], by extending collision logic to PEG-functionalized crystalline silica where current-step magnitude tracked particle size despite the particles being electrochemically inert [45], and by forming multimetallic nanoparticles from roughly 50 attoliter droplets while consuming at least 200-fold fewer metal atoms than a Pt/C benchmark catalyst [46]. Together with the observation that charge-transfer kinetics can change at free nanoparticles of only 7–15 nm radius, and that the nano effect is not identical for Ag and Au [47], these studies show how far SEE has moved beyond visibility-driven demonstrations. It now quantifies transport regime, interfacial partitioning, particle size, catalytic productivity, and even materials economy on an entity-by-entity basis.

More recent soft-entity studies also make clear that collector architecture and interfacial chemistry are part of the measurement logic. Single-nanodroplet electrochemistry has now been used to probe liquid–liquid interfacial kinetics directly in situ instead of inferring

them from ensemble transfer curves. Water nanodroplet collisions were likewise shown to depend strongly on the surrounding microelectrode insulator, making the glass sheath part of the effective sensing interface rather than an inert support [48]. Even when the droplet itself is chemically similar, the electrode material can redirect the event family: RTIL-stabilized nitrobenzene microemulsions produced distinct collision-current signatures at carbon-fiber and gold ultramicroelectrodes, showing that soft-entity readout reflects emulsion–electrode interaction kinetics as much as droplet arrival statistics [49]. The same conceptual expansion is now reaching gas entities. Off-axis dark-field microscopy resolved individual H_2 nanobubbles during electrolysis [50], while nanopore sensing pushed further to single-digit nanobubbles and extracted voltage-dependent size and diffusion behavior [51]. For analytical chemistry, the key point is that SEE can quantify transient droplets and bubbles as physically evolving interfaces, not just as nuisance signals.

Fast waveform analysis and application-facing soft-entity detection make this branch richer still. Combined fast-scan sinusoidal voltammetry with short-time Fourier transform analysis has been used to resolve disruption dynamics and charge transfer within single attoliter emulsion droplets at apparent scan rates up to 200 V s^{-1}, showing that even droplet breakup can be followed electrochemically instead of averaged away [52]. A different application-oriented study used pitting collisions to detect individual aqueous droplets in organic solvents and relate post-event pit morphology to droplet size, which is attractive analytically because the collision leaves a structural memory rather than only a fleeting current trace [53]. Together with the nanodroplet and nanobubble papers above, these studies indicate that soft-entity SEE is moving from proof-of-principle observation toward interfacial diagnostics.

Semiconducting and photoelectrochemical SEE adds another underused but analytically revealing branch. Single-nanoparticle photoelectrochemistry at a nanoparticulate TiO_2-filmed ultramicroelectrode produced sub-millisecond photocurrent transients and allowed electron diffusivity to be inferred from event-level signals rather than from an ensemble photocurrent alone [54]. A related Pt/TiO_2/n-Si platform coupled collision-style event analysis with sustained photoelectrode performance, maintaining about 19 mA cm^{-2} under 100 mW cm^{-2} illumination for more than 12 h while still resolving single-particle electron-transfer behavior [55]. Shape-controlled single-Pt nanoparticle studies strengthened the same message by correlating morphology directly with electrocatalytic activity at the entity level [56]. Together, these papers show that SEE is not confined to metallic impacts or ionic blockades; it can also quantify how local semiconductor architecture, optical excitation, and nanoparticle geometry modulate the analytical readout.

Electrochemical imaging of single semiconducting particles is also becoming more quantitative and more local. Superlocalization analysis of cobalt-oxide particles resolved activation-associated size changes with precision down to about 20 nm, making it possible to connect optical trajectory and electrochemical state in the same entity-level experiment [57]. A complementary picked-and-dropped strategy then placed individual Co_3O_4 nanoparticles onto the tip of a carbon nanoelectrode and measured oxygen-evolution current densities up to 11.5 A cm^{-2} with turnover frequencies of 532 $\pm$ 100 s^{-1} at 1.92 V versus RHE [58]. Together these studies show that SEE can now interrogate semiconducting and oxide catalysts not only in stochastic collision mode, but also through operando optical tracking and deliberately immobilized single-particle measurements.

Single-particle spectroelectrochemistry is pushing that integration even further by treating optical line shape and electrochemical activity as simultaneous descriptors of the same entity. Oxygen-plasma treatment enhanced H_2O_2 electrocatalysis of individual Au nanorods without grossly deforming their morphology, showing that one can improve activity while still preserving the spectral identity needed for single-particle correlation [59].

A related study on 1,2-benzenedithiol-modified Au nanorods used electrochemical control to resolve chemical-interface damping at the single-particle level, demonstrating that ligand-induced plasmon broadening can itself become an electroanalytical observable [60]. More recently, electrochemical surface engineering was used to generate Cu and Cu_xS on individual Au nanorods and thereby strengthen nitroaromatic electrocatalysis under plasmonic tracking [61]. These papers are analytically useful because they convert optical spectroscopy from mere visualization into a co-equal event-assignment channel for single-particle electrochemistry.

Importantly, this spectroelectrochemical logic did not appear all at once. Earlier work already showed that thiophenol-passivated Au nanorods can be driven electrochemically to tune chemical-interface damping while the plasmonic response is tracked at the single-particle level, providing a bridge between simple optical monitoring and the more elaborate activity-correlation studies that followed [62]. The broader analytical point is that linewidth, damping, and catalytic response are becoming coupled observables rather than separate characterization tasks.

The second major class is confinement-enabled SEE, encompassing nanopores, nanopipettes, nanocavities, recessed nanoelectrodes, and related architectures in which transport is restricted before or during signal generation. Here the analytical advantage is not only smaller capacitance but also selective control over capture, residence time, and local concentration [2,63,64]. Nanopores are especially important because they blur the boundary between electrochemistry, sensing, and single-molecule biophysics. Cai et al. [2] demonstrated an electro-optical nanopore binding assay in which synchronized ionic-current and fluorescence signals enabled selective small-molecule and protein recognition at the single-event level, with reported detection down to the sub-picomolar regime for certain targets. More recently, Zhou et al. [13] extended solid-state nanopores to ex situ single-cell protein analysis, using nanopipette-based extraction followed by single-molecule readout from cellular contents. These studies illustrate why confinement is central to the molecular frontier: rather than waiting for a small analyte to produce a measurable faradaic response in open solution, the interface is engineered so that even a brief passage event carries enough informational density to justify single-entity assignment.

The third class comprises proximal interrogation platforms such as nanoelectrodes, nanocapillaries, and electrochemical probes inserted near or into complex targets. These tools are particularly important for single-cell work because they decouple entity isolation from stochastic arrival. Instead of waiting for an analyte to collide with a detector, the detector is brought to the relevant subcellular space [9,65,66]. The best-known realization is single-cell amperometry, where a carbon-fiber microelectrode positioned at a cell surface records individual exocytotic spikes. Trouillon and Ewing showed that even the cell surface glycocalyx modulates those spike shapes, meaning that the electrochemical readout captures not only secretion chemistry but also the nanomechanics of the release environment [3]. This example is analytically instructive: the same transient can be both a readout of analyte quantity and a reporter of the local cellular interface. Such coupling increases scientific richness but makes direct comparison across studies more difficult unless geometry and biological context are explicitly controlled.

The fourth class is imaging-enabled or multiplexed SEE, where arrays or optical coupling transform isolated transients into spatially or statistically richer datasets. Wang et al. [4] used plasmonic electrochemical impedance microscopy to visualize single-cell processes label-free, extending the concept of entity-resolved electrochemistry beyond current transients toward spatially resolved impedance maps. Alden et al. [6] recently pushed high-throughput SEE with automated microelectrode arrays, recording 3270 single-particle collision events from 671 electrodes within a few hours and then using

deep-learning-assisted analysis to extract event-size distributions. Figure 4 places these device-enabled and imaging-based formats alongside localized nanoelectrode architectures, making clear that modern SEE is no longer defined by one canonical electrode geometry. The comparison is analytically important because each architecture improves a different bottleneck: arrays increase event statistics, imaging restores spatial context, and proximal probes trade stochastic capture for deliberate access to the interface of interest.

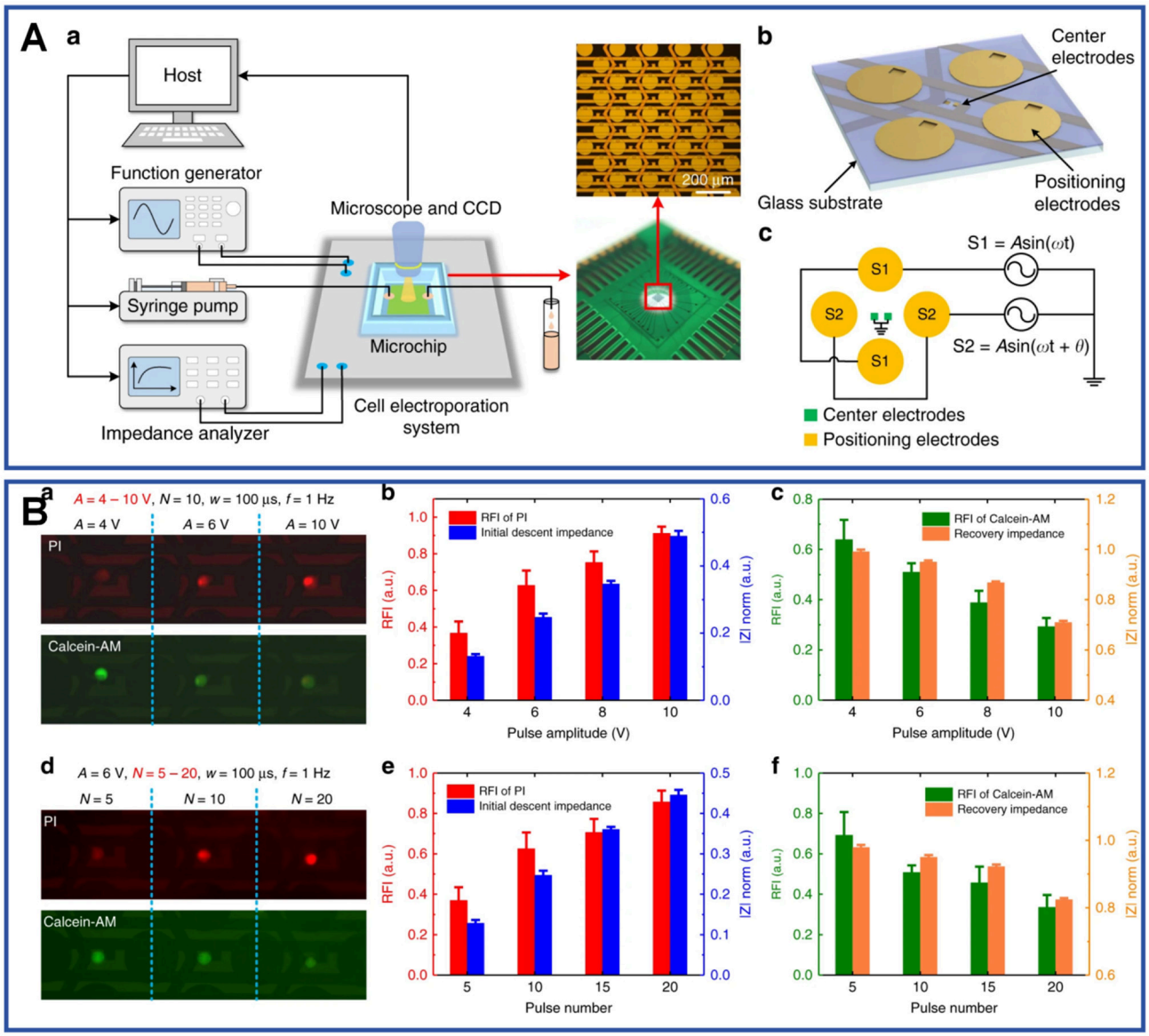


Figure 4. Nanoelectrodes, electrochemical imaging, and device-enabled SEE architectures. (**Aa**) Sketch of the electroporation system with a microelectrode array chip. (**Ab**) Schematic view of the microelectrode unit on the chip. (**Ac**) Signal application mode for cell positioning. (**Ba**) Fluorescent images of PI and Calcein-AM for HeLa cell electroporation at different pulse amplitudes. (**Bb**) Relative fluorescence intensity (RFI) of PI and initial descent impedance at different pulse amplitudes. (**Bc**) Relative fluorescence intensity of Calcein-AM and recovery impedance at different pulse amplitudes. (**Bd**) Fluorescent images of PI and Calcein-AM for HeLa cell electroporation for different pulse numbers. (**Be**) Relative fluorescence intensity of PI and initial descent impedance for different pulse numbers. (**Bf**) Relative fluorescence intensity of Calcein-AM and recovery impedance for different pulse numbers. Adapted from [67] under the terms of the Creative Commons Attribution License.

The platform diversity summarized in Figures 3 and 4 is a strength, but it also creates a comparability problem. Collision platforms excel at event counts and at probing catalytic nanoparticles, yet often struggle with mechanistic uniqueness. Nanopore systems can approach molecular specificity, but their throughput and quantitative calibration vary strongly with pore geometry, surface chemistry, and data-analysis strategy. Proximal probes provide unmatched cellular context at the expense of invasiveness and standardization. Imaging and arrays offer statistical depth, but sometimes at the cost of the intimate time resolution that made SEE distinctive in the first place [5,6,64]. A critical review must therefore resist the temptation to treat all entity-resolved electrochemical measurements as analytically equivalent simply because they observe one event at a time.

One useful way to see these differences is to ask what each platform class treats as its main scarce resource. In collision electrochemistry, the scarce resource is often event identity: once the experiment is stable, it may be possible to gather many transients, but extracting a unique particle property from each one remains difficult unless catalytic chemistry or surface design constrains the inverse problem. In nanopore systems, the scarce resource is usually neither events nor raw current amplitude, but rather interpretable dwell time and event-class separation. This is why a top sensing pore of about 2 nm, a lower-layer pore count ranging from 1 to 9, or a sampling rate of 50–100 kHz matters analytically rather than merely instrumentally [8,13,64]. In intracellular and proximal-probe systems, by contrast, the scarce resource is often experimental reproducibility under physical perturbation of the sample. A 500 nm aperture with a near-Nernstian response, a 4 × 4 chip with >95% viability, or a nanokit with <10 fL local delivery can therefore be more analytically significant than a marginal gain in nominal spatial resolution [66–68]. Framing the field this way helps explain why no single transduction architecture is likely to dominate SEE as a whole.

2.3. Analytical Metrics, Confidence Criteria, and Data Treatment

Because SEE operates near the limit where signal, noise, and interpretation become inseparable, analytical metrics must be broader than the conventional triplet of sensitivity, selectivity, and limit of detection. At least six dimensions matter repeatedly across the literature: current or charge amplitude, temporal resolution, event capture efficiency, assignment confidence, throughput, and calibration strategy [6,69]. Current amplitude determines whether an event is even visible; temporal resolution determines whether short-lived events survive instrumental filtering; capture efficiency governs how many real entities are missed; assignment confidence determines how many detected events are genuine; throughput controls the statistical reliability of inferred distributions; and calibration determines whether an observed signal can be translated into quantity rather than merely compared qualitatively.

The field has historically overemphasized the first two of these dimensions. Many papers quite reasonably celebrate picoampere or sub-picoampere event detection and millisecond or sub-millisecond time resolution. Yet such claims alone do not guarantee meaningful analytics. In high-throughput microelectrode-array SEE, for example, Alden et al. [6] showed that large event numbers can change the quality of inference itself because distributions become more stable and amenable to data-driven classification. In single-cell amperometry, by contrast, a well-resolved spike may still be analytically incomplete if the cell count is low or if release fractions are discussed without corresponding vesicle-content measurements [3,7]. For near-single-molecule nanopore sensing, specificity may depend more on synchronized or orthogonal readouts than

on absolute current depth, as Cai et al. [2] demonstrated with combined electrical and optical detection.

This is why confidence of assignment should be elevated to a first-class analytical metric. A single transient is never self-interpreting. It becomes evidence only when alternative origins are systematically narrowed. Confinement, chemical recognition, event-shape analysis, orthogonal optical validation, and mechanistic control experiments all increase confidence, but none is universally sufficient. The exocytosis modeling work of Dannaoui et al. [70] makes this point well: seemingly similar amperometric spikes can encode different physical release mechanisms, so fitting and interpretation must be grounded in explicit transport models rather than informal visual comparison. In other words, SEE data analysis increasingly requires the same rigor that the field has long applied to hardware development. To make this criterion operational within the main text, assignment confidence can be reported as a transparent 0–3 judgment. A score of 0 indicates that the event origin is not supported beyond event visibility; 1 indicates model-based assignment with limited controls; 2 indicates support from recognition chemistry, orthogonal validation, or mismatch/buffer controls; and 3 should be reserved for convergent evidence that also reports quantitative denominators such as false-assignment rate, rejected events, insertion success, capture efficiency, and analyzable-event fraction. The same ordinal logic is used for event-throughput and effective-yield comparisons. A low score denotes that the denominator is absent or limited to a single trace, an intermediate score denotes replicate event or cell counts and an analyzable fraction where available, and the strongest score is reserved for reports that distinguish rejected, silent, and successful events or provide array-based or automated data with statistically meaningful denominators. The scale is therefore not a universal performance number; it records how much evidence each report provides for event capture, assignment, and quantitative reproducibility.

Another underappreciated metric is practical readiness, by which we mean whether a platform can be transferred across operators, laboratories, and sample types without losing interpretability. Some SEE configurations are analytically elegant but depend on fragile fabrication, manual probe placement, or idiosyncratic data-processing pipelines. Others are less spectacular in headline sensitivity yet more reproducible because they are array-based, automated, or coupled to explicit statistical workflows [6,67]. This tension between ultimate sensitivity and operational robustness will recur throughout the review and becomes central in Section 5, where the field is benchmarked directly across platforms. For now, the key point is that the enabling toolbox of SEE should be judged by how well it balances localization, event visibility, interpretability, and reproducibility.

These criteria establish the analytical lens used in the rest of this review. Sections 3 and 4 examine how specific platforms perform when the target becomes either a single molecule or a single cell. Section 5 extends this comparison across platforms by identifying which combinations of architecture, signal processing, and experimental design most credibly move electrochemistry toward its ultimate detection limits without sacrificing quantitative meaning.

3. Moving Towards Detecting Single Molecules

3.1. Direct Stochastic Detection of Redox-Active Molecules

Single-molecule electrochemistry has long occupied a special place in the imagination of the field because it appears to represent the ultimate sensitivity limit of an interfacial electrical measurement. Yet the literature makes clear that “single-molecule detection” is not a single experimental category. Historically, the most direct routes emerged from studies of electron transfer through molecular junctions, electrochemical scanning tunneling

microscopy, and highly localized electrochemical environments, where one seeks to observe the response of an individual molecule or of a very small and explicitly countable molecular population [14,71,72]. A landmark example was the early nanogap SECM-style experiment that used an approximately 15 nm tip separated from the substrate by about 10 nm to detect ferrocene derivatives as stochastic current bursts, showing that electrochemical detection can indeed approach the one-molecule limit under tightly engineered geometry [71]. These studies were foundational because they showed that electron transfer can be interrogated at essentially molecular dimensions. However, they were rarely analytical in the modern sense, because throughput was low, calibration was difficult, and the assignment of one electrical trace to one analyte species often depended on highly controlled interfaces rather than realistic sample matrices.

The current analytical frontier is therefore dominated less by classical faradaic single-molecule measurements than by stochastic event sensing in confined ionic-current systems. Here, the signal is not necessarily the direct oxidation or reduction current of one molecule. Instead, the molecule perturbs an electrochemically maintained ionic flux through a nanopore or nanogap, and the perturbation is interpreted as a single-entity event. This shift is not a conceptual retreat. On the contrary, it reflects a practical recognition that molecular-scale electroanalysis becomes more credible when the interface is engineered to boost information density per event rather than when one insists on measuring vanishingly small faradaic currents in open solution [2,63,64]. The transition was accelerated by biological nanopore work in which transport was actively structured rather than merely observed; for example, a mutant MspA pore coupled to phi29 polymerase delivered median current-level durations of about 28 ms and current differences up to 40 pA between neighboring sequence states, demonstrating that single-molecule electroanalysis becomes far more powerful once dwell time and state separability are co-designed [73]. The result is a family of platforms that often look more like nanopore biophysics than traditional electroanalysis, yet remain electrochemical at their core because the measurement relies on current flow, interfacial control, and electrically driven transport.

Several recent primary studies illustrate how far this logic has progressed. Cai et al. [2] developed a single-molecule electro-optical binding assay using nanopores, coupling ionic current readout with synchronized fluorescence so that electrical events could be assigned with substantially greater confidence than would be possible from current blockades alone. Ahmad et al. [8] then generalized protein detection at single-molecule precision by engineering a modular protein nanopore whose analyte-specific recognition element sits at the pore entrance rather than inside the pore lumen, thereby reducing steric restrictions while preserving event specificity. In a different direction, Cui et al. [74] used a cyclodextrin-functionalized α-hemolysin system to discriminate duloxetine enantiomers from their single-molecule blockade characteristics, showing that nanoscale confinement can resolve differences too subtle for many ensemble electrochemical readouts. Taken together, these studies reveal a defining feature of modern single-molecule electrochemistry: the analyte itself is rarely enough. Chemical recognition, confinement, or an orthogonal channel of validation is typically required before a transient becomes analytically convincing.

Another sign of analytical maturation is that the target is no longer only molecular identity, but also molecular integrity and dynamic state. Single-molecule nanopore sensing has now been applied to RNA degradation analysis, extending event-based electroanalysis from binding or sequence-state discrimination toward the assessment of RNA quality itself [75]. This matters because conventional integrity workflows often depend on ensemble gel-based assays with substantial material demand, whereas nanopore readouts can

in principle interrogate degradation statistics one molecule at a time. The implication is broader than RNA alone: once SEE can quantify how an analyte changes, not just whether it is present, the gap between single-molecule electroanalysis and practical bioanalysis narrows appreciably.

This does not mean direct molecular electrochemistry is analytically obsolete. Instead, it means that directness should be judged functionally rather than dogmatically. If a molecule produces a unique, interpretable, and quantifiable event under a controlled electrochemical bias, the measurement advances the single-molecule goal even when the signal is an ionic blockade rather than a classical faradaic pulse. The more important analytical issue is whether the platform can distinguish specific from nonspecific events, quantify rare targets against the background, and retain meaning when moved beyond idealized buffers. Regarding that test, the studies assembled in Table 1 already show the contours of a quantitative design space rather than a simple sensitivity race. Electrocatalytic amplification made 4.2 nm Pt nanoparticle collisions observable with signal gains exceeding 10 orders of magnitude [1], whereas single-particle monitoring of Au-surface self-assembly used 60 pM nanoparticles, found a minimum collision current of about 37 pA at 730 nM 6-MCH, and extracted a diffusion-controlled adsorption constant of 3.97×10^6 L mol^{-1} for the rapid assembly stage [16]. In confined single-molecule sensing, the strongest papers increasingly report affinity and bandwidth together: Cai et al. [2] reached apparent K_d values of 7.6 ± 1.2 pM for streptavidin and 3.7 ± 0.2 pM for cDNA with a 0.1 pM limit of detection, whereas Ahmad et al. [8] resolved two EGFR-bound states with K_D values of 181 ± 8 nM and 34 ± 2 nM at 50 kHz sampling and 10 kHz filtering. These apparent K_d/K_D values should be read as platform-specific, condition-dependent estimates rather than as directly comparable thermodynamic constants, because confinement, transport, recognition chemistry, and event-classification rules differ across studies. These gains are real, but they are delivered by increasingly elaborate control of recognition, transport, and event assignment rather than by raw current minimization alone.

Table 1. Cross-study quantitative comparison of representative SEE reports on molecules, proteins, and nanoscale particles, with explicit citation numbers and assignment-confidence basis alongside amplification mode, confinement strategy, kinetic window, conditions, and quantitative analytical output.

Entity Class	Analytical Target	Platform	Core Quantitative Data	Conditions or Geometry	Assignment-Confidence Basis	Reference
single nanoparticles	electrocatalytic collision amplification	Pt nanoparticle collisions at an ultramicroelectrode	Pt nanoparticles as small as 4.2 nm were detected, and electrocatalytic amplification produced signals more than 10 orders of magnitude larger than the direct oxidation current expected from a single nanoparticle.	Collision signal was amplified through catalytic reaction at the electrode rather than direct nanoparticle oxidation.	Electrocatalytic amplification with size and concentration logic.	[1]
single nanoparticles	catalytic IrO_x collision transients	$NaBH_4$-treated Pt ultramicroelectrode	The transient signal consisted of repeated current spikes superimposed on a current decay; spike frequency was directly proportional to particle concentration, and peak current increased with applied potential.	Surface conditioning of the Pt UME was essential for reproducible blip-type responses.	Concentration-dependent blip frequency and potential response.	[15]
single nanoparticles	ultralow concentration analysis by timing statistics	5 um Pt ultramicroelectrode with 1 um particles	Experiments were performed with 1 um particles at 0.145, 1.45, and 14.5 fM, with at least 10 replicate experiments per concentration to compare first-arrival-time statistics against full collision counting.	Time to first detectable event was used as the quantitative observable.	First-arrival statistics with at least 10 replicates.	[5]
single nanoparticles	surface-chemistry-dependent collision kinetics	single-nanoparticle electrochemical collision at a carbon-fiber microelectrode	The assay used 60 pM Au nanoparticles and varied 6-MCH concentration from 0.73 pM to 73 uM, corresponding to C_6-MCH/CAuNP ratios from 1.2×10^{-2} to 1.2×10^{6}; the average collision current reached a minimum of about 37 pA at 730 nM 6-MCH (ratio 1.2×10^{4}); the rapid adsorption stage followed a diffusion-controlled Langmuir model with $k_a = 3.97 \times 10^{6}$ L mol^{-1}.	The study compared bare, 6-MCH-modified, and MCH-modified Au nanoparticles during self-assembly in solution.	Surface-chemistry controls and Langmuir adsorption fit.	[16]
single nanoparticles	comparison of signal-amplification chemistries	10 um carbon ultramicroelectrode collision sensing	Representative systems were 4.8 ± 0.5 nm Pt nanoparticles in hydrazine, 15 ± 2 nm Au nanoparticles in HCl, and 20 ± 2 nm Ag nanoparticles in H_2O_2, all measured by electrocatalytic amplification at a 10 um carbon UME.	The paper juxtaposed several catalytic chemistries under the same collision-amplification logic.	Parallel catalytic chemistries under the same collision logic.	[17]
single nanoparticles	kinetics of hydrazine oxidation at the single-entity level	graphene oxide-supported Pd nanoparticle impact voltammetry	The impact-voltammetry method resolved hydrazine oxidation kinetics across pH 2–11 and showed that both N_2H_4 and $N_2H_5^+$ are electroactive, with the rate-determining step assigned as a one-electron transfer under Butler–Volmer behavior.	Single-particle events were used to infer electrocatalytic kinetics rather than merely to detect particle presence.	pH-dependent impact voltammetry and Butler–Volmer kinetic fit.	[11]
single molecules	synchronized electro-optical nanopore binding assay	nanopore with correlated optical and electrical readout	For streptavidin binding, the carrier concentration was 10 pM and streptavidin was titrated from 0 to 100 pM, giving $85.7 \pm 2.2\%$ synchronized events at two-fold excess and an apparent K_d of 7.6 ± 1.2 pM; for cDNA, K_d was 3.7 ± 0.2 pM with a 0.1 pM detection limit; for thrombin, K_d was 5.0 ± 0.4 nM with a 0.5 nM detection limit.	Electrical blockade events were matched to optical signatures from the same entities.	Orthogonal optical-electrical synchronization and mismatch controls.	[2]

Table 1. *Cont.*

Entity Class	Analytical Target	Platform	Core Quantitative Data	Conditions or Geometry	Assignment-Confidence Basis	Reference
single proteins	state-resolved protein biomarker sensing	engineered tFhuA protein nanopore	The tFhuA pore had average internal diameters of about 2.6 and 3.9 nm; EGFR binding produced two substates with K_D values of 181 ± 8 nM and 34 ± 2 nM, open-state current of 18.2 ± 0.1 pA, and blocked-state currents of 6.4 ± 0.1 and 2.3 ± 0.1 pA at +20 mV; recordings were sampled at 50 kHz and filtered at 10 kHz.	Pore engineering enabled state-specific recognition of a protein target.	Engineered recognition element and state-resolved dwell/current classes.	[8]
single molecules	translocation control through coupled nanopores	bilayer coupled nanopore system	The top 2D sensing pore was about 2 nm; the number of pores in the lower guiding layer was varied from one to nine; representative 2D pore sizes included about 0.85 × 0.85 nm, 1.7 × 1.3 nm, 1.29 × 1.47 nm, 1.81 × 1.89 nm, and 2.17 × 3.15 nm; readout operated with microsecond-scale temporal resolution.	Transport was slowed and spatially organized by coupling pores across layers.	Defined pore geometry and transport-control design.	[64]
single chiral molecules	enantioselective molecular recognition	functionalized alpha-hemolysin nanopore with SBEbetaCD receptor	Duloxetine enantiomers were discriminated in an alpha-hemolysin receptor whose constriction, barrel, and vestibule diameters are about 14, 22, and 26 A, respectively; the duloxetine dynamic diameter spans about 4.47–8.67 A; the platform was also used to determine enantiomeric excess of duloxetine mixtures.	Chiral recognition chemistry was integrated into a nanopore readout using alpha-HL and sulfobutyl ether-beta-cyclodextrin.	Recognition chemistry with enantiomer-specific blockade distributions.	[74]
single molecules	glycoprotein affinity interactions in confinement	4-MPBA-functionalized nanopipette nanopore	A single IgG molecule was translocated through a 4-MPBA-modified nanopipette under bias to generate distinguishable blockade events; statistical analysis yielded an equilibrium association constant k_a, and the confined single-molecule k_a was reported to be much larger than the ensemble open-system value.	Confinement and boronate chemistry were combined in a nanopipette format using IgG as the model glycoprotein.	Boronate recognition plus blockade-event statistics.	[76]
single molecules	coordination kinetics under nanoconfinement	K_{238}H-AeL reactive nanopore	Each pore carried seven histidine residues at the 238 position, and the confined nanopore increased the bonding rate constant of Au(III)-histidine coordination by about 10–100 times relative to bulk solution while also defining an optimal applied voltage for the single-molecule reaction.	Reactive histidine sites and nearby carboxylate groups were positioned inside a biological nanopore to study Au(III) coordination.	Engineered histidine sites with voltage-dependent kinetic fitting.	[77]
single proteins from cell-derived samples	protein detection with solid-state nanopores	12 ± 2 nm SiNx membrane with 8.64 and 8.84 nm pores	Representative current peaks were 6.44 nA for 293T cell lysate and 1.70 and 6.67 nA for purified controls; data were collected at 100 kHz and low-pass filtered at 10 kHz.	Single-molecule protein sensing was extended to cell-derived extracts rather than ideal purified buffers only.	Cell-lysate versus purified-control comparison; sampling/filter stated.	[13]
single nanoparticles	distance-dependent stochastic collisions	SECM monitoring of IrO_x nanoparticle collisions	Collision frequency versus distance followed the theoretical negative-feedback SECM approach curve at high mediator concentration, demonstrating that single-particle collision counting can reproduce ensemble mass-transport behavior.	SECM tip-substrate distance was varied during stochastic collision measurements.	SECM approach-curve agreement with mass-transport theory.	[18]

Table 1. *Cont.*

Entity Class	Analytical Target	Platform	Core Quantitative Data	Conditions or Geometry	Assignment-Confidence Basis	Reference
single nanoparticles and nanoelectrodes	formation of a tunneling ultramicroelectrode by single-particle contact	Pt UME/TiO_2/Pt nanoparticle tunneling electrode	A TiO_2 film was deposited until the ferrocenemethanol oxidation wave just disappeared, and a single Pt nanoparticle collision restored electron transfer to solution species through tunneling, producing an nm-scale active area with long-term stability.	Single-particle contact was used not only as an event to count but as a route to fabricate a functional nanoelectrode.	Single-particle contact restores tunneling-mediated electron transfer.	[19]
single nanoparticles	facet-dependent oxygen evolution catalysis	single-particle Co_3O_4 collision electrochemistry	Cubic Co_3O_4 nanoparticles of 8.7 ± 1.2 nm showed average onset potential and overpotential values of about 1.78 and 0.40 V, whereas spheroidal particles of 9.6 ± 1.4 nm showed about 1.93 and 0.56 V, respectively.	Shape-controlled single nanoparticles were compared one by one for OER activity.	Shape-controlled particles with OER activity comparisons.	[21]
single nanoparticles	plasmon-enhanced electrocatalysis at the single-entity level	nanoimpact electrochemistry under optical excitation	The study used glucose electrooxidation and oxygen reduction on gold nanoparticles as model reactions and showed that, unlike ensemble photocurrent measurements, plasmonic effects dominated the single-entity photocurrent response under SEE conditions.	Optical excitation was integrated with collision electrochemistry on suspended gold nanoparticles.	Optical excitation versus dark electrocatalytic controls.	[20]
single soft nanoparticles	electrocatalytic turnover on individual soft particles	single-particle electrocatalysis with vitamin B_{12} mediator	Single Vitamin B_{12}-containing droplets were used to catalyze trichloroethylene dehalogenation, and the turnover number was quantified at the individual soft-particle level; kinetic analysis showed chemically reversible binding of TCE to the electro-reduced Co(I) state.	Soft nanoparticle catalysis was analyzed one particle at a time rather than by bulk turnover averages.	Single-droplet turnover with kinetic model support.	[30]

3.2. Amplified and Confinement-Assisted Strategies

Confinement-assisted strategies have become the dominant route toward practical single-molecule electroanalysis because they address two problems at once: they increase local interaction probability and they slow or reshape transport so that events survive the bandwidth limits of measurement electronics. Studies based on nanopore electrodes, pressure-regulated carbon nanopipettes, electro-optical readout, and coupled nanopores show that nanogaps, nanopores, and recessed geometries do not merely miniaturize experiments but alter the very physics of transport and reaction so that rare events become measurable [2,63,64,78]. In this sense, confinement is an analytical amplifier even when no chemical amplification reagent is used.

The route to modern transport-engineered nanopores can now be traced through a coherent primary-literature lineage rather than inferred retrospectively. Double-barrel nanopores first showed that dual-pore geometry can modulate single-molecule dwell behavior and thereby turn transport control into an adjustable experimental parameter [79]. A separate edge-field-leakage strategy slowed short single-stranded DNA translocation through solid-state nanopores by up to five orders of magnitude and enabled discrimination of duplexes with 97% confidence [80], while polymer-transport studies clarified that event distributions under drive follow transport physics and scaling laws rather than reflecting pore geometry alone [81]. On the application side, oligodeoxynucleotide-labeled nanopore mapping resolved neighboring genomic sites separated by 141 bp, or about 48 nm, showing that transport-controlled single-molecule readout can support spatially meaningful mapping rather than only yes-or-no detection [82]. Active dual-solid-state nanopore control subsequently extended this logic to bacterial-genome mapping under feedback-guided motion [83]. These studies sit close to nanofluidics and biophysics, but analytically they are central to SEE because they convert transport from a nuisance variable into a tunable source of specificity and confidence.

The experimental embodiments of this idea are increasingly sophisticated. Chou et al. [64] recently introduced coupled bilayer nanopores in which one layer guides and decelerates the molecule while the second 2D nanopore senses it, producing distinct T-shaped and W-shaped translocation signals that encode positional information and fragment length at microsecond resolution. This is an important advance because it addresses a classic weakness of single-molecule event analysis: if a molecule translocates too rapidly, the event is detected but poorly characterized. By redesigning the transport path rather than merely smoothing the electronics, coupled nanopores increase both dwell time and interpretability [84]. Yang et al. [77] used confinement to probe single-molecule coordination kinetics, demonstrating that nanoconfined ionic-current fingerprints can expose dynamic binding processes that are nearly inaccessible in bulk assays. Zhou et al. [13] pushed the concept further into an analytically relevant biological context by detecting proteins at the single-molecule level directly from material harvested from single cells, thereby linking molecular sensitivity to cellular heterogeneity rather than treating them as separate problems.

A closely related recent study in Matter extended the coupled-pore logic to tracking and detecting unmodified molecules in bilayer-coupled nanopores, reinforcing that transport engineering has become a reproducible design principle rather than a one-off device trick [85]. Direct single-entity protein electrochemistry is also beginning to re-enter this discussion from the faradaic side. A catalase study on carbon-fiber ultramicroelectrodes reported a 0.57–16.98 pM linear range and analyzed 572 spikes with a geometry-aware theoretical model, showing that entity-resolved protein electrochemistry can now be framed quantitatively rather than only phenomenologically [86]. Together, these papers help

bridge the old divide between nanopore-style indirect sensing and direct electrochemical protein detection.

Not all amplification strategies rely on purely physical confinement. Chemical amplification, catalytic cycling, or recognition-mediated dwell-time enhancement can also transform barely resolvable events into usable single-molecule signals. Tang et al. [76] showed that a boronic-acid-functionalized nanopore can recognize glycoproteins at the single-molecule level, where the critical variable is not simply the magnitude of a current blockade but the chemically programmed interaction between the analyte and the pore interior. Cui et al. [74] similarly relied on a bionic recognition receptor to turn subtle chiral differences into separable blockade features. A conceptually different but analytically important route was shown by Pt nanoparticle electrochemical amplification for DNA analysis, where a 31-base target sequence was translated into a single-label response through 20-base detection and 16-base capture probes, making collision-style amplification useful for biomolecular recognition rather than only catalytic nanoparticles [86]. These studies are analytically instructive because they remind us that amplification in SEE is often informational rather than just electrical: a longer dwell time, a more distinctive multilevel event, or a more constrained interaction pathway can be as valuable as a larger current amplitude. Taken together, these studies resolve into four recurring routes toward single-molecule electroanalysis, summarized in Figure 5: direct redox event capture, confinement-enhanced capture, chemically programmed recognition, and hybrid multimodal detection.

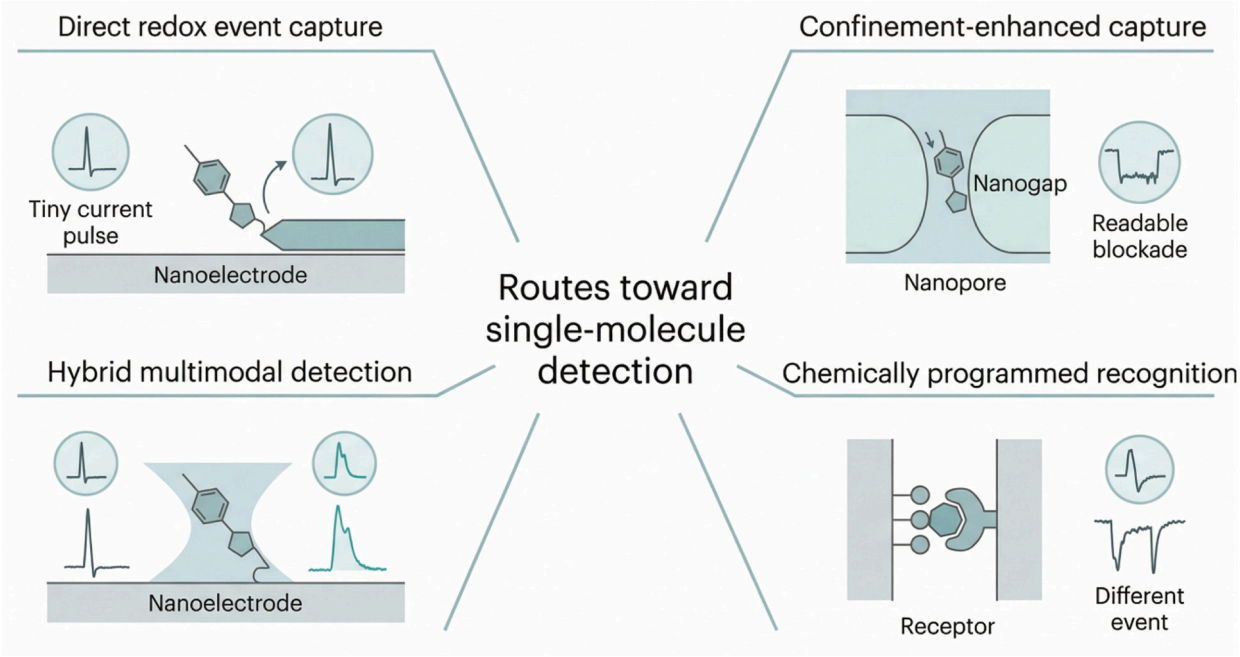


Figure 5. Mechanistic comparison of direct, confined, catalytic, and hybrid electrochemical routes toward single-molecule detection.

Figure 6 makes that distinction concrete by juxtaposing electro-optical and engineered-protein nanopore systems. In Cai et al. [2], synchronized optical and electrical readout turned rare capture events into quantifiable affinity measurements, whereas Ahmad et al. [8] used an engineered protein pore to separate EGFR-bound substates through distinct current levels and dwell-time classes. The analytical commonality is that specificity emerges from structured event families rather than from translocation alone.

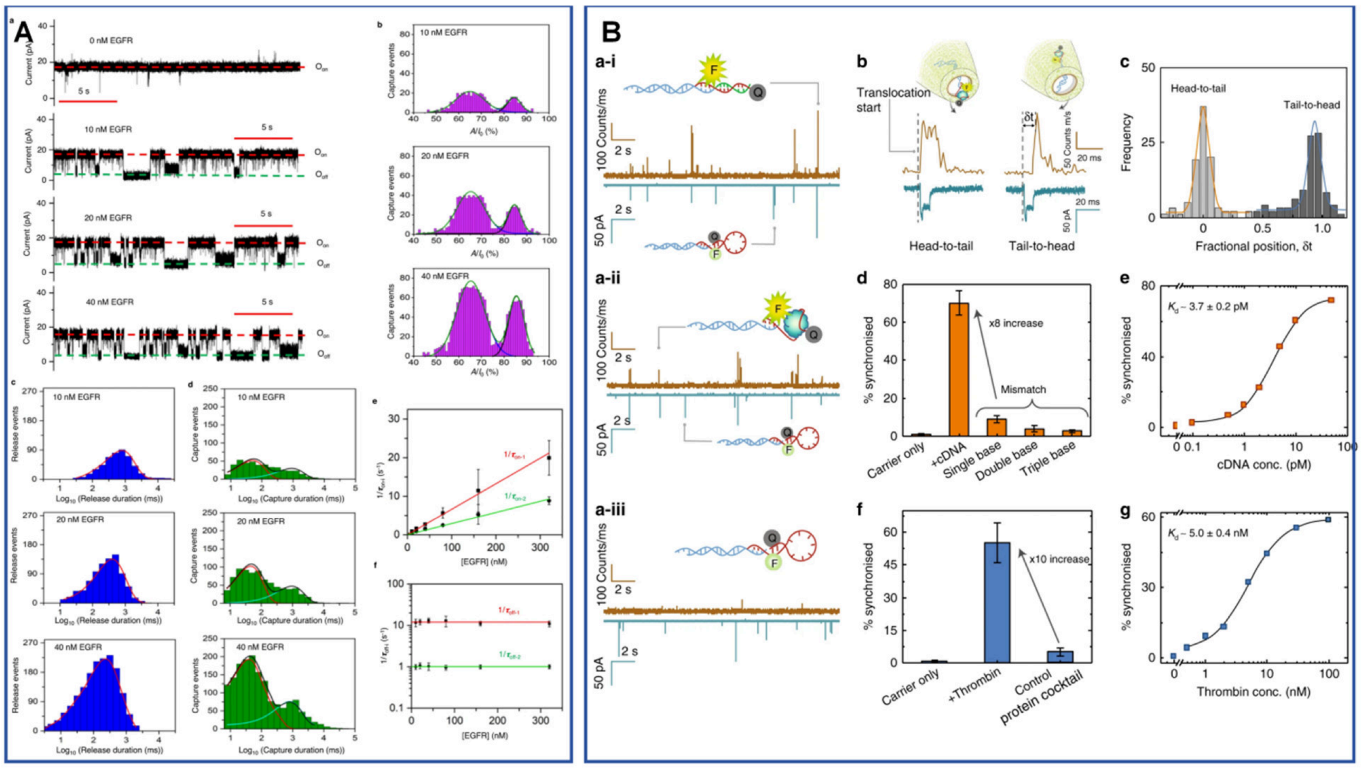


Figure 6. Direct or near-direct single-molecule electrochemical events. (**Aa**) Single-channel traces (in black) of Adnectin1-tFhuA in the presence of EGFR. (**Ab**) Event histograms (in magenta) of the normalized current blockades A/I_0, where A and I_0 are the amplitude of blockades and the amplitude of the open substate, respectively. (**Ac**) Histograms (in blue) of the EGFR-released durations (τ_{on}) at various EGFR concentrations, [EGFR]. (**Ad**) Histograms (in green) of EGFR-captured durations (τ_{off}) at different [EGFR]. (**Ae**) Dependence of the event frequencies in the form of $1/\tau_{on\text{-}i}$ on [EGFR]. (**Af**) Dependence of $1/\tau_{off\text{-}i}$ on [EGFR]. (**B**) Detection of DNA oligos and proteins using molecular beacons. Photon and current time traces are shown for the translocation of (**Bai**) DNA MB-Carrier-cDNA, (**Baii**) DNA MB-Carrier-Thrombin, and (**Baiii**) DNA MB-Carrier. (**Bb**) Orientation of the complex translocating through the nanopore was determined by characterizing the (**Bc**) fractional position for the onset of the optical signal relative to the onset of the electrical signal (N = 193). (**Bd**) Percent synchronization between the optical and electrical channels for cDNA bound to the MB-Carrier along with controls including single, double, and triple base mismatches. (**Be**) A binding affinity of 3.7 pM was calculated by fitting a Hill binding model for cDNA as a function of % synchronization. (**Bf**) Percent synchronization between the optical and electrical channels for thrombin bound to the MB-Carrier along with controls. (**Bg**) A binding affinity of 5.0 nM was calculated by fitting a Hill binding model for thrombin as a function of % synchronization, which agreed with existing bulk methods. Adapted from [2,8] under the terms of the Creative Commons Attribution License.

3.3. Critical Barriers to Routine Single-Molecule Electroanalysis

Despite impressive demonstrations, the field remains well short of routine single-molecule electroanalysis in the same way that single-cell amperometry became routine for exocytosis. The first reason is event ambiguity. Even in highly engineered nanopore systems, blockade depth and dwell time can be influenced by access resistance, surface charge, conformational variability, pore-to-pore heterogeneity, and non-specific adsorption. Specific recognition reduces this ambiguity but can also introduce new complications such as multistate binding, slow regeneration, or sensitivity to matrix components [8,64,74]. A convincing single-molecule claim therefore requires more than rare-event observation; it requires a robust argument that alternative origins have been excluded and that event classes remain separable as concentrations, buffers, or sample complexity change.

The second barrier is calibration. In ensemble analytical chemistry, calibration curves are conceptually straightforward even when experimentally laborious. In single-molecule electrochemistry, the relevant variables often include not just concentration but also capture probability, electric-field geometry, binding kinetics, and the fraction of analytes that produce interpretable events. Cai et al. [2] improved this situation by using an orthogonal optical channel to validate electrical events, whereas Chou et al. [64] improved it by redesigning transport to produce more structured signal shapes. Yet the broader problem remains unresolved: translating event frequency and waveform distributions into absolute molecular counts still depends heavily on platform-specific models. Without explicit handling of capture efficiency and silent events, a claim of single-molecule sensitivity can drift into a claim of single-molecule detectability under favorable circumstances rather than robust quantitation.

What Table 1 makes clear is that the calibration problem is not uniform across molecular SEE platforms. In electro-optical nanopores, one can at least tie event classes to apparent affinity constants and formal detection limits, as Cai et al. [2] did with K_d values of 7.6 ± 1.2 pM and 3.7 ± 0.2 pM and limits of detection down to 0.1 pM. In engineered protein nanopores, the problem shifts toward assigning bound substates and extracting state-resolved constants, as reflected in the 181 ± 8 nM and 34 ± 2 nM K_D values for EGFR binding in tFhuA [8]. In receptor-programmed or confinement-strengthened systems such as glycoprotein-recognition nanopipettes and chiral nanopores, the measurable variable may instead be an apparent enhancement in interaction strength relative to open solution or a reproducible difference in event family between two closely related analytes [74,85]. These are analytically legitimate outcomes, but they are not interchangeable. A future standard for single-molecule SEE should therefore require authors to state explicitly whether their calibration targets concentration, binding affinity, event classification confidence, or transport control. Too many papers still imply that one metric stands in for all of them.

The third barrier is throughput. Molecular event detection is often technically exquisite but statistically thin. This matters because at the single-molecule limit, variability is not noise to be averaged away; it is the signal one hopes to interpret. A platform that records only dozens of events may be enough for mechanistic proof-of-concept but not for reliable quantification in heterogeneous samples. The contrast with array-enabled SEE is instructive. High-throughput single-particle collision studies now routinely generate thousands of events [6], whereas many single-molecule studies still depend on limited event populations. Bridging that gap will require multiplexed nanopore recording, more stable interfaces, and analysis pipelines that can classify complex event families without overfitting.

This contrast also helps explain why collision electrochemistry and nanopore electrochemistry have evolved different notions of maturity. Collision studies can often accumulate event-rich distributions quickly, but each event may carry relatively modest chemical specificity unless the interface or catalyst has been engineered very carefully. Nanopore studies can deliver much richer event-level identity information, yet they often pay for that richness with lower practical throughput, more elaborate models of transport and binding, and greater sensitivity to pore-to-pore variation. The field should resist treating these modes as if they were simply different implementations of the same assay. They occupy different points in an analytical trade-off space between event number, event complexity, and assignment confidence. This is precisely why array-scale collision workflows and confinement-engineered molecular workflows should be benchmarked side by side rather than forced into a single best-performance hierarchy [5,6,8,64].

Finally, there is a conceptual barrier: many of the most informative molecular demonstrations are hybrid measurements that sit at the interface of electrochemistry, nanofluidics, and molecular recognition. This hybridity is a strength, not a weakness, but it means that progress should be assessed by analytical outcome rather than by whether the signal looks traditionally electrochemical. The key issue is not perfect reproduction of classical voltammetric logic at one-molecule scales. The key issue is whether electrochemically controlled interfaces can deliver selective, quantitative, reproducible, and eventually high-throughput molecular analytics in real samples. Current studies indicate that this goal is most likely to be approached through chemically intelligent confinement and multimodal validation rather than through direct current-amplitude minimization alone.

4. Moving Towards Detecting Single Cells

4.1. Vesicle Release and Exocytosis

Single-cell electrochemistry is the most mature branch of SEE because it couples a well-defined electroactive analyte class, catecholamines and related transmitters, to an experimentally accessible biological event, exocytosis. Single-cell amperometry remains the archetype: a carbon-fiber microelectrode placed at the cell surface converts quantal release into current spikes whose peak amplitude, half-width, and integrated charge report release dynamics and vesicular content. What makes this subfield analytically powerful is that its central signal, the amperometric spike, is both chemically meaningful and statistically abundant. Hundreds of events can often be collected from a single experiment, making heterogeneity part of the observable rather than an inconvenient source of noise [3,70].

Exocytosis studies have also taught the field a crucial lesson: a single-cell electrochemical transient is rarely a simple proxy for "more" or "less" analyte. Trouillon and Ewing demonstrated that the glycocalyx at the cell surface modulates exocytotic spike shapes, meaning that the recorded event reflects not only vesicular release but also the nanostructured environment through which the released molecules diffuse [3]. Ye et al. [7] showed that combining single-cell amperometry with intracellular vesicle impact electrochemical cytometry can separate vesicle content from released fraction, revealing pharmacological effects that would have been missed if spike charge alone had been interpreted as secretion efficiency. Dannaoui et al. [70] underscored the importance of explicit transport modeling by linking spike shapes to release-fusion scenarios instead of treating all spikes as phenomenologically interchangeable. The same conclusion is no longer confined to one cell type or recording geometry. Intracellular nanomeasurements in living neurons revealed subquantal and chemically complex exocytosis, reinforcing the view that release fraction must be defined at the vesicle level, not inferred from released charge alone [87]. Complementary modeling of cylindrical enzymatic nanoelectrodes for transient exocytosis detection likewise showed that probe geometry and enzyme-layer design can reshape the measured waveform before any biological interpretation is made [88]. Single-cell electrochemistry has therefore become one of the clearest examples in analytical chemistry of mechanistic modeling and quantitative readout having to evolve together.

Vesicle electrochemical cytometry and its intracellular variants make that requirement especially concrete because the analytical numerator, counted molecules, is inseparable from how completely a vesicle opens at the electrode. Early mechanistic work showed that isolated chromaffin vesicles release only about one-tenth as much catecholamine as intact cells and that vesicle rupture probability rises strongly as temperature increases from 6 to 30 °C, directly tying event yield to membrane mechanics rather than analyte concentration alone [89]. That insight was sharpened when geometry-specific VIEC experiments

showed that a 33 um flat disk electrode can oxidize essentially 100% of vesicular catecholamine, whereas a conical nanotip with 4 um length and 1.5 um base diameter recovered only about 75% unless the vesicle opening formed close to the nanopore [90]. More recently, repeated-and-partial-release VIEC paired resistive pulses with electrochemical charge to obtain 278 synchronous size-content measurements, reporting a median vesicle radius of 216 nm, a median content of 2.64×10^6 catecholamine molecules, and an intravesicular concentration of 0.101 M; about 96% of 340 vesicles still opened within 5 s, but only a subset showed a second measurable pulse, indicating that repeated release is real without being universal [91]. IVIEC has also become sensitive to membrane remodeling chemistry: carbon-nanotube treatment increased vesicle content from 2.25×10^6 to 3.88×10^6 molecules and raised vesicle volume by about 50%, supporting fusion-driven storage enhancement rather than a trivial change in oxidation efficiency [92].

These vesicle-level tools are now moving from methodological demonstrations to chemically specific biology and tissue analysis. Primary studies have shown that intravesicular chemistry is tunable: replacing control media with 100 uM potassium salts for 30 s followed by 30 mM KCl depolarization altered vesicular storage and exocytotic release in an anion-dependent manner, implicating ion-specific effects in monoamine packing and release fraction [93]. Natural-product modulation has likewise become measurable at the vesicle level; single-vesicle electrochemistry showed that polysaccharide treatment increased vesicular dopamine storage while also enhancing exocytotic release in PC_{12} cells [94]. Membrane-composition perturbations can be resolved even more directly: single-vesicle microelectroanalysis identified phosphatidylinositol 4,5-bisphosphate as a regulator of vesicle opening dynamics and linked lipid composition to the balance between storage and release [95]. Synaptic vesicle electrochemistry has now been extended to fresh brain slices, enabling in situ quantification of vesicular monoamine instead of relying only on cultured-cell surrogates [96]. A 2026 study then combined IVIEC with single-cell amperometry in fresh brain slices and isolated neurons to mimic the clinical administration of oxaliplatin, showing that single-vesicle electrochemistry can interrogate drug-induced remodeling of vesicular storage and release in near-physiological tissue contexts [97].

Figure 7 captures this shift by juxtaposing classic spike-based measurements with newer modeling-driven interpretations. The field's progress is evident, but so is its complexity: high-quality single-cell electrochemistry does not just count spikes; it interprets how many molecules were stored, how many were released, how fast the fusion pore evolved, and how the cell-surface architecture altered the electrochemical signature. The quantitative spread assembled in Table 2 makes that point concrete. Trouillon and Ewing observed 395 spikes from 12 control cells, 646 spikes from 15 neuraminidase-treated cells, and only 108 spikes from 12 protamine-treated cells, with a 2.2× increase in surface dopamine diffusion after glycocalyx removal [3]. In beta cells, matched SCA and IVIEC measurements yielded $39{,}317 \pm 1611$ stored serotonin molecules versus $13{,}310 \pm 1127$ released molecules per vesicle, making partial release numerically unavoidable rather than merely qualitative [98]. At the isolated-vesicle level, RP-VIEC added 278 synchronous size-content pairs and estimated a median intravesicular concentration of 0.101 M, showing that molecule counting and vesicle sizing can be experimentally coupled instead of inferred separately [91]. Meanwhile, intracellular ion and physicochemical probes are beginning to provide calibration-grade numbers of their own, such as the 56.6 mV per decade chloride response over 5–100 mM with an about 500 nm nanopipette aperture and a 120 ms response time [66]. These examples justify comparing Table 2 studies not only by signal size, but also by the kind of biological heterogeneity each platform can quantify reproducibly.

Table 2. Cross-study quantitative comparison of representative single-cell and subcellular electrochemical studies, highlighting sample size, event yield, molecular counts, temporal response, heterogeneity resolved, and the assignment-confidence basis for each cited study.

Cell or Subcellular Target	Analyte or Process	Platform	Core Quantitative Data	Conditions or Geometry	Reference	Assignment-Confidence Basis
single cells	exocytosis kinetics and glycocalyx effects	carbon-fiber single-cell amperometry	Control: 12 cells and 395 peaks; neuraminidase: 15 cells and 646 peaks; protamine: 12 cells and 108 peaks; surface dopamine diffusion was 2.2× faster after neuraminidase; the cell-surface diffusion coefficient was at most 45% of the free-solution value.	Surface glycans were perturbed before SCA recording.	[3]	Perturbation groups with cell and spike counts.
single cells and vesicles	lidocaine-dependent exocytosis versus vesicle content	SCA plus IVIEC	Coupled SCA and IVIEC showed biphasic lidocaine effects: at relatively high lidocaine concentration the fusion pore became narrower and longer-lasting with less monoamine released than control cells, whereas at relatively low concentration the pore stayed open even longer and released more monoamine than control cells; IVIEC confirmed that vesicle catecholamine content did not change.	Single-cell amperometry was paired with intracellular vesicle impact electrochemical cytometry in the same biological context.	[7]	Paired SCA and IVIEC comparison in the same biological context.
single cells and vesicles	mechanistic fitting of exocytotic spike shapes	single-cell amperometry plus theory	More than 50–80% of spikes belonged to the common class; one representative data set was 84% analyzable with 97 double-exponential and 9 single-exponential spikes; fitted D_{ves}/r_{ves}^2 values were 415 s^{-1} for chromaffin cells and 5.8 × 10^3 s^{-1} for PC12 cells; fitted vesicle radii were 156 nm and 95 nm, respectively; fitted $r_{pore,max}$ values were 20 nm and 12 nm.	HEPES buffer; 5 um carbon-fiber electrode; +680 mV versus Ag/AgCl; 105 mM K^+ puff stimulation; model explored vesicle radii of 80–300 nm and cell-electrode gaps of 100–200 nm.	[70]	Model class assignment with analyzable-event fraction.
single cells	label-free electrical imaging of cell processes	plasmonic electrochemical impedance microscopy	The method reached submicrometer spatial resolution and millisecond temporal resolution and was sensitive enough to resolve ion-channel activities with conductances of about 2 pS.	Plasmonic EIM converted impedance changes into optical intensity maps at the single-cell level.	[4]	Label-free imaging with spatial, temporal, and conductance metrics.
single cells	individualized electroporation with impedance tracking	4 × 4 addressable microelectrode array chip	The chip integrated a 4 × 4 microelectrode array and achieved more than 95% cell viability together with more than 95% transfection efficiency; single-cell positioning was completed within 30 s and impedance recovery typically reached a stable level after about 200–300 s.	Array-addressable single-cell handling was combined with electroporation and impedance tracking on the same device.	[67]	Array addressing plus viability, transfection, and recovery metrics.
single cells	intracellular chloride sensing	hollow Ag/AgCl nanopipette nanoelectrode	The hollow Ag/AgCl nanoelectrode had an about 500 nm aperture, responded within 120 ms, and showed a Nernstian slope of 56.6 mV per decade over a 5–100 mM chloride range.	Probe geometry and response were optimized for intracellular insertion into single cells.	[66]	Calibrated Nernstian slope, response time, and probe geometry.
single cells	intracellular wireless bipolar electrochemiluminescence analysis	nanopipette-confined bipolar ECL	The Pt-decorated nanopipette enabled intracellular measurement of hydrogen peroxide and glucose concentrations as well as sphingomyelinase activity in vivo, while keeping the applied potential spatially confined inside the nanopipette to minimize perturbation of cellular activity.	Nanopipette confinement was used to localize the intracellular analytical circuit and generate luminol ECL.	[10]	Nanopipette confinement localizes the intracellular ECL circuit.

Table 2. *Cont.*

Cell or Subcellular Target	Analyte or Process	Platform	Core Quantitative Data	Conditions or Geometry	Reference	Assignment-Confidence Basis
single cells	dual intracellular ROS and temperature sensing	bifunctional Pt/Ni nanoprobe	After Al_2O_3 insulation the probe diameter expanded to approximately 500 nm; after FIB milling the limiting current was about 0.25 nA; H_2O_2 response was linear over 0.08–1.28 mM; temperature calibration was linear from 294.15 to 320.15 K.	Bifunctional nanoprobe for simultaneous chemical and thermal intracellular readout.	[9]	Dual chemical and thermal calibration ranges on the same probe.
single neurons	subquantal release and complex exocytosis	nanoelectrochemical intracellular measurements	The abstract reports that 65.4% of events showed partial release and that only 37.2% of vesicular content was released on average; the remaining 34.6% of events were full-release events.	Intracellular nanoelectrochemical measurements were used in living neurons.	[87]	Partial/full-release classification with percentage denominators.
single-cell nucleus	hydrogen peroxide in nucleus versus cytoplasm	self-referenced nanopipette with Pt ring tip	The self-referenced design confined the applied potential inside the capillary and demonstrated that, under oxidative stress, the amount of H_2O_2 measured in the nucleus was lower than that in the cytoplasm of the same single living cell.	Self-referenced nanopipette inserted into nucleus and cytoplasm of the same cell.	[99]	Self-referenced nuclear/cytoplasmic comparison in the same cell.
single beta cells	vesicle content versus released serotonin	nanoscale amperometry plus IVIEC	Average stored serotonin was 39,317 ± 1611 molecules per vesicle whereas average released serotonin was 13,310 ± 1127 molecules; the data set included 26 SCA cells and 51 IVIEC cells in the abstracted summary.	Matched comparison of release output and vesicle content in beta cells.	[98]	Matched stored-versus-released molecule counts across cell groups.
single living cells	intracellular glucose and sphingomyelinase analysis	nanokit capillary with Pt ring electrode	The capillary had an opening of about 130 nm and an outer Pt-coated diameter of about 200–300 nm after insulation; the limiting current was about 1 nA; optimum ejection used 1 V for 2 s with an ejected volume below 10 fL covering about a 3 um region; glucose was detected from 0.05 to 5 mM with RSD below 9.04%; average intracellular glucose was estimated at about 2 mM from a mean single-cell charge of 0.44 nC.	One capillary integrated delivery, aspiration, and electrochemical detection for intracellular analysis.	[68]	Delivery volume, calibration range, and single-cell charge estimate.
single cells	target-triggered assembly inside a nanopipette	ATP-responsive aptamer nanopipette	The nanopipette used ATP-dependent split-aptamer assembly on a Au-coated interior wall to increase surface charge density and enhance the rectification signal; the platform was reported as sensitive, rapid, selective, stable, and highly recyclable for intracellular ATP analysis.	Nanostructure assembly was driven by intracellular ATP chemistry inside the pipette volume.	[100]	ATP-triggered recognition chemistry inside the nanopipette.
single cells	collision discrimination of cancer and healthy cells	microelectrode collision method	Upon single-cell collisions in the presence of surfactant, the electrochemical response of acute lymphoblastic lymphoma T-cells differed by two orders of magnitude from that of healthy thymocytes.	Whole-cell collisions were read through consumption of intracellular electroactive contents at the microelectrode.	[101]	Two-order current contrast between cancer and healthy cells.
single synapses	dopamine release plasticity during repetitive stimulation	carbon-fiber nanoelectrodes	Repeated stimulation left event frequency and maximal dI/dt essentially unchanged, but vesicle opening duration increased by 73.8% and release amount increased 1.4-fold; adjacent release sites were about 45 nm apart on average.	Carbon-fiber nanoelectrodes monitored dopamine exocytosis at synaptic release sites under repetitive stimulation.	[102]	Synaptic-site measurements with repeated-stimulation denominators.

Table 2. *Cont.*

Cell or Subcellular Target	Analyte or Process	Platform	Core Quantitative Data	Conditions or Geometry	Reference	Assignment-Confidence Basis
single vesicles	repeated and partial release with coupled size-content readout	resistive pulses in nanopores plus VIEC	The study reported 278 synchronous size-content measurements, a median vesicle radius of 216 nm, a median catecholamine content of 2.64×10^6 molecules, and a median intravesicular concentration of 0.101 M; about 96% of 340 vesicles opened within 5 s.	Resistive-pulse sizing and amperometric molecule counting were measured from the same vesicle population.	[91]	Synchronous resistive-pulse sizing and amperometric molecule counting.
single intracellular vesicles	carbon-nanotube-induced fusion and storage enhancement	IVIEC	Carbon-nanotube treatment increased vesicle volume by about 50% and raised the median catecholamine content from 2.25×10^6 to 3.88×10^6 molecules per vesicle.	Intracellular vesicle impact electrochemical cytometry was used before and after CNT exposure.	[92]	Before/after CNT exposure with vesicle volume and content shifts.
single cells	cytoplasmic microviscosity	twin nanopipettes	The platform reported an average cytoplasmic microviscosity of about 86 cP in MCF-7 cells and resolved drug-induced shifts after cytoskeleton perturbation.	Twin nanopipettes were used for real-time electrochemical monitoring of intracellular physical-state changes.	[103]	Twin-nanopipette microviscosity calibration in live cells.
single human platelets	serotonin quantification and platelet counting	collision SEE at ultramicroelectrodes	Single-platelet collision peaks were integrated to determine serotonin concentration while collision frequency provided platelet counts.	Platelets isolated from human blood collided with an ultramicroelectrode and generated anodic current peaks via serotonin oxidation.	[104]	Platelet collision frequency and serotonin charge integration.

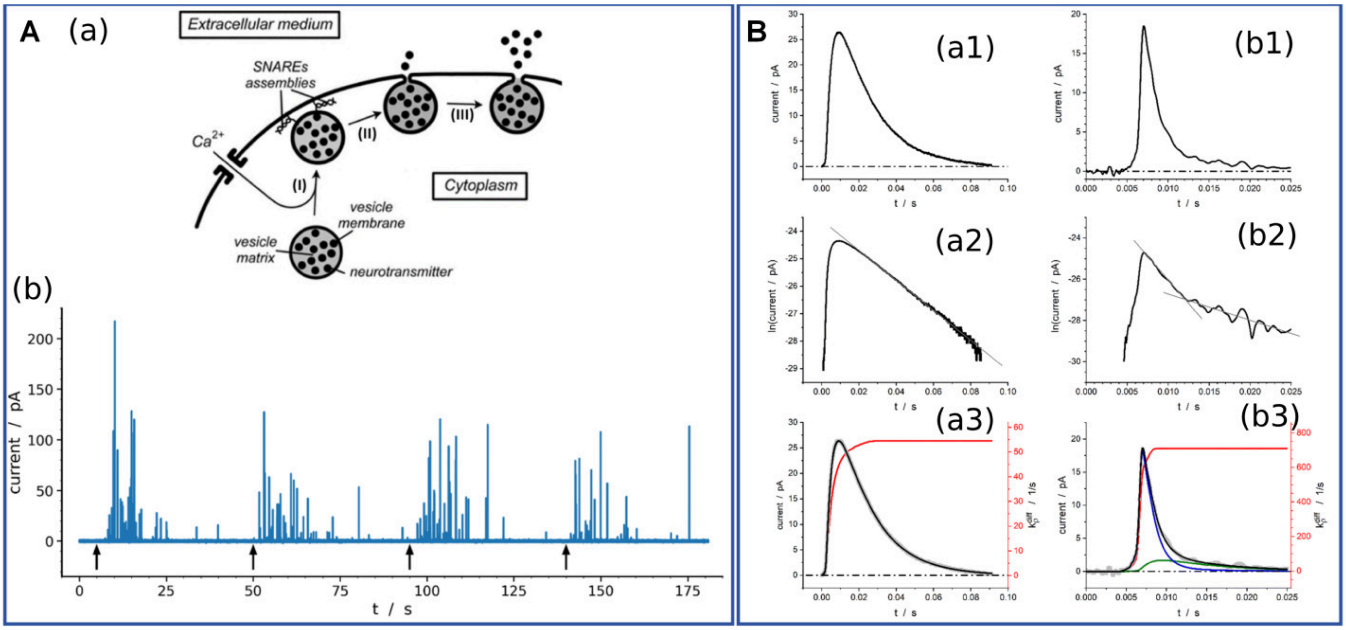


Figure 7. Illustration of vesicle release, exocytotic spike analysis, and fusion-pore dynamics. (**Aa**) Schematic representation of the main exocytotic release steps. (**Ab**) Representative amperometric data from a single PC12 cell with highly loaded vesicles recorded in HEPES buffer with 5 µm carbon-fiber electrode held at +680 mV vs. Ag/AgCl. (**B**) Single ((**a1**–**a3**)) and double exponential ((**b1**–**b3**)) spikes in linear (1) and semi-log (2) scales; shows simulations results of the spike current (black), its components. Adapted from [70] under the terms of the Creative Commons Attribution License.

Subcellular electrochemistry sharpens that lesson further. Monitoring individual exocytotic events inside a single synapse showed that the relevant analytical unit can be smaller than the whole cell and that the acceptable trade-off between invasiveness and information content changes accordingly [105]. More recently, repetitive-stimulation studies at synaptic release sites found that vesicle opening duration increased by 73.8% and released amount by 1.4-fold, even while event frequency and maximal dI/dt remained nearly unchanged; the same work estimated adjacent release sites to be only about 45 nm apart [102]. These results matter well beyond neurochemistry. They show that once the analytical unit shifts from the cell to the synapse or vesicle, the decisive variable may no longer be average secretion output but nanoscale plasticity in release architecture. For SEE, this is both a triumph and a warning: the field can now resolve increasingly subtle biological heterogeneity, but only if the probe geometry, sampling denominator, and interpretive model are reported with enough detail to make those distinctions credible.

4.2. Intracellular and Cell-Surface Electrochemical Interrogation

The next frontier is to move from watching what leaves the cell to measuring what happens inside it. This transition is analytically challenging because intracellular electrochemistry must balance spatial precision, invasiveness, calibration, and temporal resolution under conditions where perturbing the cell can easily change the quantity one hopes to measure. Primary studies using nanowires, nanopipettes, and multifunctional nanoprobes have expanded the accessible target space from classical neurotransmitters to reactive oxygen and nitrogen species, chloride, and local physicochemical parameters [9,65,66]. Yet they also show that intracellular electroanalysis remains far less standardized than exocytosis measurements.

Recent primary studies reveal both the promise and the fragility of this area. Zhang et al. [66] reported a hollow Ag/AgCl nanopipette nanoelectrode system that

combines localized iontophoretic infusion with single-cell chloride sensing, allowing intracellular chloride to be perturbed and read out on the same platform. Ma et al. [9] developed a bifunctional nanoprobe capable of simultaneous intracellular ROS and temperature detection, highlighting a broader trend toward multimodal intracellular electroanalysis rather than one-analyte-one-probe designs. Wang et al. [10] earlier demonstrated wireless intracellular analysis using a bipolar electrochemiluminescence strategy inside a nanopipette, illustrating that electrochemical single-cell interrogation can be coupled to optical reporting rather than relying solely on faradaic current collection. Other primary studies broaden the chemical reach further but also expose how variable current assay design still is. Self-referenced nanopipette measurements of nuclear H_2O_2 showed that even subcellular compartments such as the nucleus can be addressed electrochemically [99], while target-triggered assembly inside nanopipettes showed that intracellular recognition chemistry can be used to gate signal generation rather than merely report passive concentration change [100]. These studies collectively suggest that the most successful intracellular platforms are no longer those that minimize probe size alone, but those that couple localization with a clear strategy for calibration and interpretability.

Recent work also shows that intracellular electrochemistry is expanding from concentration measurements to local physical-state and metal-ion readout. Twin nanopipettes were used for real-time monitoring of cytoplasmic microviscosity, reporting an average value of about 86 cP in MCF-7 cells and resolving shifts after cytoskeleton-perturbing drugs, which means the electrochemical probe was effectively sensing intracellular rheology rather than only a chemical concentration [103]. A separate nanopipette platform extended electrochemical sensing to Cu^{2+} analysis in vitro and in vivo, indicating that biologically relevant metal ions are becoming tractable single-cell or near-cell electrochemical targets rather than being left to optical chelators alone [106]. These studies reinforce a point that is easy to miss when the field is discussed only through ROS and neurotransmitters: the real frontier is not a longer list of analytes, but a broader definition of what a localized electrochemical measurement inside living matter can quantify.

Related micropipette work is also pushing these measurements beyond cultured-cell interiors toward living tissues and more reproducible fabrication. An ion-selective micropipette sensor using crown-ether-encapsulated MOF subnanopores enabled selective Na^+ monitoring in the living rat brain, showing that localized ion electroanalysis can move into in vivo microenvironments rather than remaining confined to isolated-cell assays [107]. On the instrumentation side, nanopipette-based electroplated nanoelectrodes provided a route to reproducible Au, Pt, Ag, and Cu nanoelectrodes with controllable geometry, which matters because intracellular claims are only as credible as the stability and reproducibility of the interfaces that produce them [108]. These papers reinforce the idea that analytical maturity in single-cell electrochemistry depends on fabrication control and physiological deployment as much as on sensitivity.

That conclusion is strengthened by several newer primary studies that push SEE below the scale of the whole cell or beyond simple small-molecule concentration readout. Disk-shaped carbon nanoprobe platforms integrated with SICM showed that probe radius can be tuned from about 5 to 200 nm, enabling intracellular and extracellular oxygen measurements with far less disruption than classical microelectrodes [109]. Electrochemical molecule-trap sensing then moved from metabolites toward low-abundance intracellular enzymes, reporting activity down to only a few molecules in one living cell [110]. More recently, platinized open carbon nanocavity electrodes mapped ROS across proliferating, quiescent, and necrotic zones in 3D cell models with a 1 nM detection limit [111], and nanosensor studies of stress granules showed that single biomolecular condensates can themselves be treated as electroactive entities whose ROS chemistry is measurable in real

time [112]. These papers broaden the meaning of intracellular electroanalysis: the target is no longer only a dissolved analyte in cytosol, but also localized enzyme activity, tissue-like microenvironmental gradients, and membraneless organelles.

The analytical details in Table 2 reinforce this point. The chloride-sensing nanopipette of Zhang et al. [66] operated with an about 500 nm aperture, showed a 56.6 mV per decade response over 5–100 mM, and reached a 120 ms response time, which is unusually close to calibration-quality ion sensing for an inserted single-cell probe. Ma et al. [9] accepted a somewhat larger physical footprint after insulation, reaching an approximately 500 nm probe diameter, but in return obtained a linear H_2O_2 range of 0.08–1.28 mM and a temperature calibration from 294.15 to 320.15 K, with a limiting current around 0.25 nA after FIB opening. These examples show why comparisons based only on nominal tip size can be misleading: the analytically more useful probe is often the one that trades a slightly larger footprint for a more trustworthy calibration window, a more stable current baseline, or a clearer multimodal response. Conversely, intracellular platforms that remain content with qualitative before-versus-after traces may be scientifically suggestive while still falling short of analytical readiness.

The nanokit strategy developed by Li and co-workers makes the same lesson visible from a different angle. Their capillary had an opening of about 130 nm, an insulated Pt-coated outer diameter of roughly 200–300 nm, and a limiting current near 1 nA; local delivery under 1 V for 2 s expelled less than 10 fL over about 3 um and supported a glucose calibration of 0.05–5 mM, from which an average intracellular glucose concentration of about 2 mM was inferred from a mean charge of 0.44 nC [68]. This is analytically important because it shows that insertion, localized delivery, aspiration, and quantification can coexist in one platform when geometry, mass transport, and calibration are co-designed rather than optimized separately. The contrast with more fragile intracellular probes is instructive: what matters for future single-cell electroanalysis is not merely reaching the interior of the cell, but doing so in a way that preserves a defensible link between the recorded signal and a physically meaningful concentration or rate.

Cell-surface and near-cell interrogation methods provide a complementary route when full intracellular insertion is too invasive or too difficult to standardize. Wang et al. [4] used plasmonic electrochemical impedance microscopy to image single-cell processes label-free, showing that electrochemical impedance can be spatially resolved at the level of individual cells without requiring electroactive reporter release. This type of readout broadens what counts as single-cell electrochemistry: the relevant entity is still one cell, but the signal is distributed in space and time rather than concentrated into a short current spike. The strength of such platforms is context. Their weakness is that signal interpretation can become indirect, because impedance, optical contrast, or coupled luminescent signals often integrate multiple physicochemical processes at once. Figure 8 highlights this trade-off by placing intracellular insertion, near-cell impedance imaging, and hybrid nanopore imaging in the same frame: the closer SEE moves toward spatially resolved cellular context, the more its interpretive burden shifts from spike counting toward geometry-aware modeling and orthogonal validation.

One especially instructive hybrid is asymmetric nanopore electron-transfer imaging in living cells. By shrinking the active pore to about 90 nm, forcing more than 90% of the potential drop into the nanopore, and using transient bubble generation to amplify ionic current by at least 3 orders of magnitude, the method enabled intracellular NADH imaging down to about 1 pM [113]. This matters analytically because it turns nanopore confinement into a live-cell imaging strategy rather than a purely molecular-sensing format, and it makes explicit how geometry-driven amplification can trade invasiveness against calibration and spatial specificity.

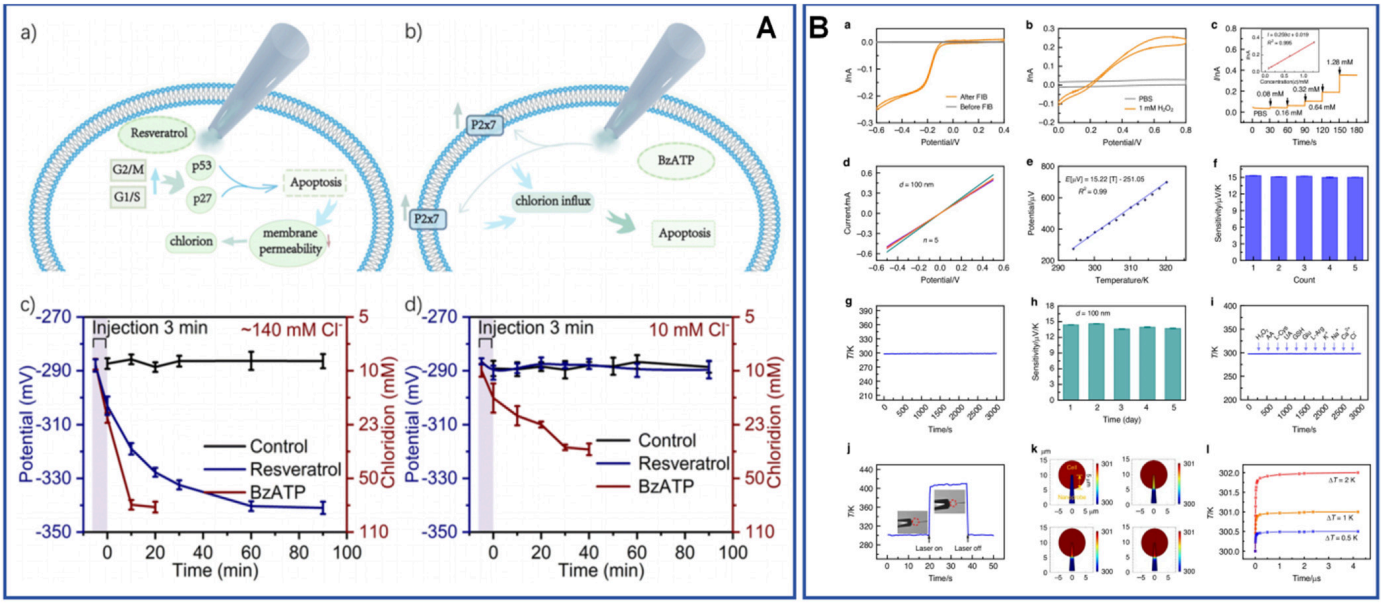


Figure 8. Illustration of intracellular and cell-surface electrochemical interrogation. (**A**) Signaling routes of (**Aa**) resveratrol and (**Ab**) BzATP-induced apoptosis. The evolution of recorded potential and corresponding intracellular chloride level in MCF-7 cells treated by electroosmotic delivery of 100 μM resveratrol and BzATP under +1 V for 3 min, with extracellular chloride set as (**Ac**) approximately 140 mM and (**Ad**) 10 mM. Error bars represent standard deviations from 10 independent detections. (**Ba**) Cyclic voltammogram of the nanoprobes in 1 mM $Ru(NH_3)_6Cl_3$/1 M KCl solution before and after FIB milling. (**Bb**) Cyclic voltammograms of the nanoprobe in 1 mM H_2O_2 solution and PBS solution. (**Bc**) Current response to varying H_2O_2 concentrations, with the corresponding calibration curve (inset). (**Bd**) I–V curves of the five individually prepared nanoprobes sputtered with a 100 nm layer of Pt and Ni in the range of −0.5 to 0.5 V in air. (**Be**) Linear voltage dependence on temperature for the nanoprobe in 10 mM PBS, within the range of 294.15–320.15 K. (**Bf**) Thermoelectric sensitivity of five individually prepared nanoprobes. (**Bg**) Stability of the nanoprobe at 298 K in 10 mM PBS. (**Bh**) Sensitivity of the same nanoprobe over five days. (**Bi**) Temperature curves of the nanoprobe in 10 mM PBS with various additives. (**Bj**) Temperature variation curve caused by laser heating at the tip. (**Bk**) Simulated transient response of the nanoprobe when the cell temperature is 1 K higher than the nanoprobe. (**Bl**) Temperature variation in the nanoprobe (5 μm away from the tip) after the nanoprobe enters the cell, with the cell temperature higher than the environment by 0.5, 1, and 2 K. Adapted from [9,66] under the terms of the Creative Commons Attribution License.

4.3. Cell Heterogeneity, Phenotyping, and Translational Relevance

For single-cell electrochemistry to matter broadly in analytical chemistry, it must do more than document exquisite individual events. It must also reveal biologically or diagnostically useful heterogeneity across populations of cells. Here, the central analytical challenge is statistical rather than purely instrumental. Single-cell measurements become valuable when they can distinguish subpopulations, treatment responses, or functional phenotypes with enough throughput and reproducibility that the distribution itself becomes the analytical result. This is why the field is increasingly moving toward arrayed devices, automated acquisition, and perturb-and-measure workflows.

Zhang et al. [67] provided an instructive example with a microelectrode-array chip that enabled individualized electroporation and real-time impedance monitoring at the single-cell level, effectively merging manipulation and readout on a device scale compatible with higher-content experiments. Lin et al. [12] more recently reported an open electrochemical-microfluidic probe that combines localized treatment and ROS detection, illustrating how single-cell electrochemistry can move toward causal phenotyping rather than passive observation alone. In such systems, the analytical endpoint is not only the magnitude of a

signal but the cell-specific response trajectory after a defined perturbation. This is exactly the type of framework required if SEE is to contribute to drug screening, stress-response analysis, or patient-derived cell phenotyping.

Here again, the quantitative details matter. The array chip of Zhang et al. [67] was not simply a clever layout; it integrated a 4 × 4 addressable architecture, completed single-cell positioning within about 30 s, maintained >95% viability and >95% transfection efficiency, and typically required only 200–300 s for impedance recovery after electroporation. Those numbers are analytically meaningful because they connect spatial selectivity to usable experimental cadence. A platform that addresses one cell at a time but needs unstable minutes or hours to recover is difficult to scale into phenotyping. By contrast, the open electrochemical-microfluidic probe of Lin et al. [12] begins to move SEE toward the logic of intervention-response assays by creating hydrodynamically confined local stimulation zones and then following ROS evolution in real time. The significance is not merely technical elegance. It is that heterogeneity becomes actionable: the measurement can distinguish how one cell responds to a controlled perturbation rather than only how cells differ at baseline.

Label-free phenotyping is also becoming more diverse in what counts as a useful cellular descriptor. Continuous single-cell phenotyping in antibody-coated microfluidic channels showed that electrochemical or impedance-style readout can be directed toward cell-surface interaction profiles rather than only soluble analytes [114]. Phase-angle-responsive light-addressable electrochemical sensing then enabled label-free imaging of single-cell adhesion across different cells and substrates, extending electrochemical single-cell analysis toward attachment mechanics and interfacial behavior [115]. An integrated single-cell array-electrochemical platform for osteogenic differentiation went a step further by enabling label-free, nondestructive longitudinal alkaline-phosphatase tracking in the same cells over time [116]. Together these studies show that "single-cell electrochemistry" is no longer synonymous only with exocytosis or ROS; it is increasingly a family of label-free phenotyping strategies.

This distinction is also why whole-cell collision studies deserve more attention in future benchmarking than they usually receive. In one early but still analytically provocative example, electrochemical collisions of acute lymphoblastic lymphoma T-cells and healthy thymocytes produced signals differing by roughly two orders of magnitude when surfactant-mediated access to intracellular electroactive content was used [101]. That result is crude compared with the mechanistic resolution of single-cell amperometry, but it captures an important translational idea: for some analytical tasks, especially rapid discrimination or screening, a lower-information but higher-contrast entity-level readout may be more useful than a highly resolved yet low-throughput intracellular trace. A mature SEE field should therefore not optimize every platform toward the same notion of richness, but should instead map each platform to the level of heterogeneity it can actually resolve with reproducible statistics.

The same logic now extends beyond mammalian cells. Label-free SEE of single living bacteria used collision-based detection of metabolically generated H_2O_2 to achieve a linear counting range from 3.0×10^7 to 1.0×10^9 cells mL^{-1}, while extracting an apparent bacterial diffusion coefficient of 6.8×10^{-9} cm^2 s^{-1} [117]. A different blocking-mode strategy distinguished E. coli and B. subtilis by combining electrochemical waveforms with fluorescence validation and reached femtomolar concentration determination [118]. These are analytically important developments because they suggest that SEE may contribute not only to neuronal or endocrine single-cell chemistry, but also to rapid microbiological counting and functional profiling where electrochemical throughput, label-free operation, and direct coupling to metabolic products are advantageous.

Clinically relevant blood components also fit this expanding bioentity view. Collision-style SEE has been used to determine serotonin concentration in single human platelets while simultaneously counting platelet events, showing that entity-level electrochemistry can address hematological targets whose clinical value lies in both chemical content and population statistics [104]. This is analytically valuable because it widens the translational case for SEE beyond cultured model cells and toward more realistic patient-facing samples.

That bacterial branch already has a clearer historical trajectory than is sometimes recognized. Early label-free collision measurements of single living E. coli reported theoretical and experimental current responses of about 75 and 83 pA, respectively, and compared predicted versus measured event frequencies on the order of 0.47 and 0.26 pM^{-1} s^{-1} [119]. Subsequent collision studies moved from counting toward species-level distinction [120], and electrochemiluminescence microscopy of individual bacteria later pushed classification accuracy to about 90.5% [121]. This progression is analytically important because it mirrors the broader trajectory of SEE itself: first make the entity visible, then make it distinguishable, and finally make it statistically classifiable in a way that supports a real analytical decision.

Yet translational relevance remains limited by three factors. First, throughput is still modest compared with optical single-cell omics or flow-based cytometry. Second, electrochemical signals are often highly informative but chemically narrow, especially when compared with transcriptomic methods. Third, standardization across probe geometry, cell handling, and analysis pipelines remains incomplete [9,12,67]. These limitations do not diminish the importance of the field; they define its comparative advantage. Electrochemical single-cell analysis is strongest when kinetics, secretion, redox chemistry, or local physicochemical state matter more than molecular breadth. Table 2 follows that premise, comparing studies not simply by sensitivity but by what form of heterogeneity they can resolve, how invasive the measurement is, and how close the platform is to reproducible analytical deployment.

5. Quantitative Benchmarking Across the Field

5.1. Sensitivity, Temporal Resolution, and Confidence of Single-Entity Assignment

The central difficulty in benchmarking SEE is that the field optimizes several incompatible goals at once. Collision electrochemistry favors event number and catalytic contrast. Nanopore-based platforms favor confinement and molecular specificity. Single-cell amperometry favors temporal fidelity for biologically meaningful transients. Imaging-enabled platforms favor context and spatial information. As a result, "best performance" depends strongly on which analytical dimension is treated as primary. Table 3 addresses this problem by separating nominal sensitivity from assignment confidence, throughput, and practical readiness rather than collapsing all performance into one ranking. Its comparison is intentionally asymmetric: 0.145–14.5 fM first-arrival nanoparticle analysis [5], 3270 events from 671 electrodes in an automated array workflow [6], 50 kHz nanopore protein-state sampling with bound-state currents of 18.2, 6.4, and 2.3 pA [8], and submicrometer or millisecond single-cell imaging with about 2 pS sensitivity [4] all count as progress, but they solve different analytical bottlenecks.

Table 3. Cross-platform benchmarking of SEE strategies approaching ultimate sensitivity, with emphasis on assignment confidence, event statistics, bandwidth, throughput, readiness for reproducible analytical deployment, and the evidence basis supporting each benchmark row.

Analytical Layer	Benchmark Focus	Platform Scale	Core quantitative Data	Benchmark Axis	Reference	Assignment-Confidence Basis
single nanoparticles	ultralow-concentration timing analysis	5 um Pt ultramicroelectrode with 1 um particles	Experiments were performed with 1 um particles at 0.145, 1.45, and 14.5 fM, with at least 10 experiments per concentration to compare first-arrival-time statistics against full collision counts.	concentration floor and analysis strategy	[5]	Replicate first-arrival analysis plus full-count comparison.
single nanoparticles	throughput and automation	microelectrode arrays and automated array microcell method	The platform characterized hundreds of electrodes with diameters from 100 nm to 2 um; collision experiments with 500 nm polystyrene beads at 2.1 um Au disk arrays yielded 3270 single-particle events from 671 electrodes in a few hours; fabrication produced 16 chips containing 3.6 K electrodes each.	throughput, arrayability, and automation readiness	[6]	3270 events from 671 electrodes; array denominator reported.
single molecules	electro-optical nanopore binding assay performance	nanopore with synchronized optical and electrical detection	For streptavidin binding the carrier concentration was 10 pM and streptavidin was titrated from 0 to 100 pM, giving 85.7 ± 2.2% synchronized events at two-fold excess and an apparent K_d of 7.6 ± 1.2 pM; for cDNA the system used 10 pM carrier plus 50 pM target, gave K_d = 3.7 ± 0.2 pM, and reached a 0.1 pM detection limit; for thrombin it used 30 nM target and gave K_d = 5.0 ± 0.4 nM with a 0.5 nM detection limit.	specificity, binding affinity, and detection limit	[2]	Synchronized optical/electrical events and mismatch controls.
single proteins	single-molecule precision protein recognition	engineered protein nanopore sensor	The tFhuA scaffold had average internal diameters of about 2.6 and 3.9 nm; for EGFR the sensor resolved two binding substates with K_D values of 181 ± 8 nM and 34 ± 2 nM, open-state current of 18.2 ± 0.1 pA, and blocked-state currents of 6.4 ± 0.1 and 2.3 ± 0.1 pA at +20 mV; electrical data were sampled at 50 kHz and low-pass filtered at 10 kHz.	specificity, state resolution, and time-resolved protein binding	[8]	Recognition element plus two resolved EGFR-bound states.
single molecules	transport control in coupled nanopores	bilayer nanopores with top 2D pore and bottom guiding pores	The top 2D sensing pore was about 2 nm; the number of pores in the bottom layer was varied from one to nine; representative drilled 2D pore sizes included about 0.85 × 0.85 nm, 1.7 × 1.3 nm, 1.29 × 1.47 nm, 1.81 × 1.89 nm, and 2.17 × 3.15 nm; the platform operated with microsecond-resolution readout.	transport control, dwell-time engineering, and positional assignment	[64]	Pore geometry and guiding-pore number explicitly controlled.
single-molecule protein detection from cell-derived samples	solid-state nanopore measurement bandwidth and signal separation	SiNx solid-state nanopore	The membrane thickness was 12 ± 2 nm; representative pore diameters were 8.64 and 8.84 nm; recordings used a 100 kHz sampling rate and a 10 kHz low-pass filter; representative current peaks were 6.44 nA for 293T cell lysate and 1.70 and 6.67 nA for purified control measurements.	bandwidth, pore geometry, and cell-derived sample compatibility	[13]	Cell-derived samples compared with purified controls; bandwidth stated.
single cells	biological-interface control of exocytosis readout	carbon-fiber single-cell amperometry	Control: 12 cells and 395 peaks; neuraminidase: 15 cells and 646 peaks; protamine: 12 cells and 108 peaks; surface dopamine diffusion was 2.2× faster after neuraminidase and the surface diffusion coefficient was at most 45% of the free-solution value.	biological variability versus instrumental variability	[3]	Perturbation groups with cell and peak denominators.

Table 3. *Cont.*

Analytical Layer	Benchmark Focus	Platform Scale	Core quantitative Data	Benchmark Axis	Reference	Assignment-Confidence Basis
single cells and vesicles	release fraction versus stored content	SCA plus IVIEC	The paired SCA-plus-IVIEC design showed that lidocaine altered fusion-pore behavior and released amount in a biphasic, concentration-dependent manner while leaving vesicle catecholamine content essentially unchanged.	measurement complementarity and interpretation of partial release	[7]	Complementary SCA/IVIEC data constrain release interpretation.
single cells and vesicles	model-based parameter extraction from spike shapes	single-cell amperometry plus mechanistic fitting	More than 50–80% of spikes belonged to the common class; a representative set contained 84% analyzable spikes, including 97 double-exponential and 9 single-exponential spikes; fitted D_{ves}/r_{ves}^2 values were 415 s^{-1} for chromaffin cells and 5.8 × 10^3 s^{-1} for PC12 cells; fitted vesicle radii were 156 and 95 nm; fitted pore radii were 20 and 12 nm.	inference depth beyond raw spike counting	[70]	Model fitting plus explicit analyzable-spike fraction.
single cells	spatiotemporal resolution of label-free electrochemical imaging	plasmonic electrochemical impedance microscopy	The method delivered submicrometer spatial resolution, millisecond time resolution, and about 2 pS ion-channel sensitivity in label-free single-cell imaging.	spatial resolution and electrical sensitivity	[4]	Optical EIM maps impedance with spatial and temporal metrics.
single cells	throughput-compatible single-cell intervention and monitoring	4 × 4 addressable microelectrode array chip	The device integrated a 4 × 4 addressable array and achieved more than 95% cell viability and more than 95% transfection efficiency while providing real-time impedance monitoring; single-cell positioning required about 30 s and impedance recovery occurred over about 200–300 s.	single-cell addressing, viability, and integration	[67]	4 × 4 array, viability, transfection, and recovery denominators.
single cells	combined perturbation and ROS monitoring	open electrochemical-microfluidic probe	The OEMP created a hydrodynamic flow-confinement area for precise local stimulation, then monitored ROS electrochemically in real time; the same platform was expanded to create symmetric subcellular treatment zones for partial membrane damage and wound-repair tracking.	integration of actuation and readout	[12]	Localized stimulation with real-time ROS monitoring.
single nanoparticles	mechanistic benchmarking of impact electrochemistry	graphene oxide platelets randomly decorated with Pd nanoparticles	The impact-voltammetry method resolved hydrazine oxidation kinetics across pH 2–11 and showed that both N_2H_4 and $N_2H_5^+$ are electroactive with Butler–Volmer kinetics; the rate-determining step was deduced to be a one-electron step.	mechanistic richness rather than concentration sensitivity	[11]	pH-dependent impact voltammetry and kinetic mechanism assignment.
single cells	intracellular multifunctional analysis geometry	nanokit capillary with Pt ring	The capillary had an about 130 nm opening and a Pt-coated outer diameter of about 200–300 nm after insulation; limiting current was about 1 nA; optimum kit ejection used 1 V for 2 s with less than 10 fL expelled over about 3 um; intracellular glucose averaged about 2 mM from a mean charge of 0.44 nC.	geometric multifunctionality	[68]	Geometry, delivery volume, and calibration window specified.
single cells	calibrated intracellular ion-sensing benchmark	hollow Ag/AgCl nanopipette nanoelectrode	The hollow Ag/AgCl nanoelectrode had an about 500 nm aperture, showed a 56.6 mV per decade response over 5–100 mM chloride, and responded within 120 ms.	calibration-ready single-cell ion sensing	[66]	Nernstian response, aperture, range, and response time specified.
single cells	dual-mode intracellular calibration benchmark	bifunctional Pt/Ni nanoprobe	After Al_2O_3 insulation the probe diameter was approximately 500 nm; after FIB milling the limiting current was about 0.25 nA; the H_2O_2 response was linear from 0.08 to 1.28 mM and the temperature response was linear from 294.15 to 320.15 K.	multimodal intracellular calibration	[9]	Dual calibration for H_2O_2 and temperature.

Figure 9 translates this tabular benchmark into a visual trade-off map by placing representative strategies along the event-throughput/effective-yield and assignment-confidence axes, while using bubble size to denote the complexity of the entity or process being assigned. The distribution of points should be read as an interpretive guide rather than as a universal ranking: high-yield array collision platforms, recognition-engineered nanopores, and single-cell or vesicle assays occupy different regions because each relieves a different bottleneck. This visualization therefore reinforces the main message of Table 3: credible SEE benchmarking must state whether a study primarily improves event statistics, event identity, or biologically interpretable context. Supplementary Table S1 provides the exact row-level values used for each plotted study and reports the platform-category means used in panel B; the sensitivity flags in that table identify score assignments that would be most affected by a stricter threshold.

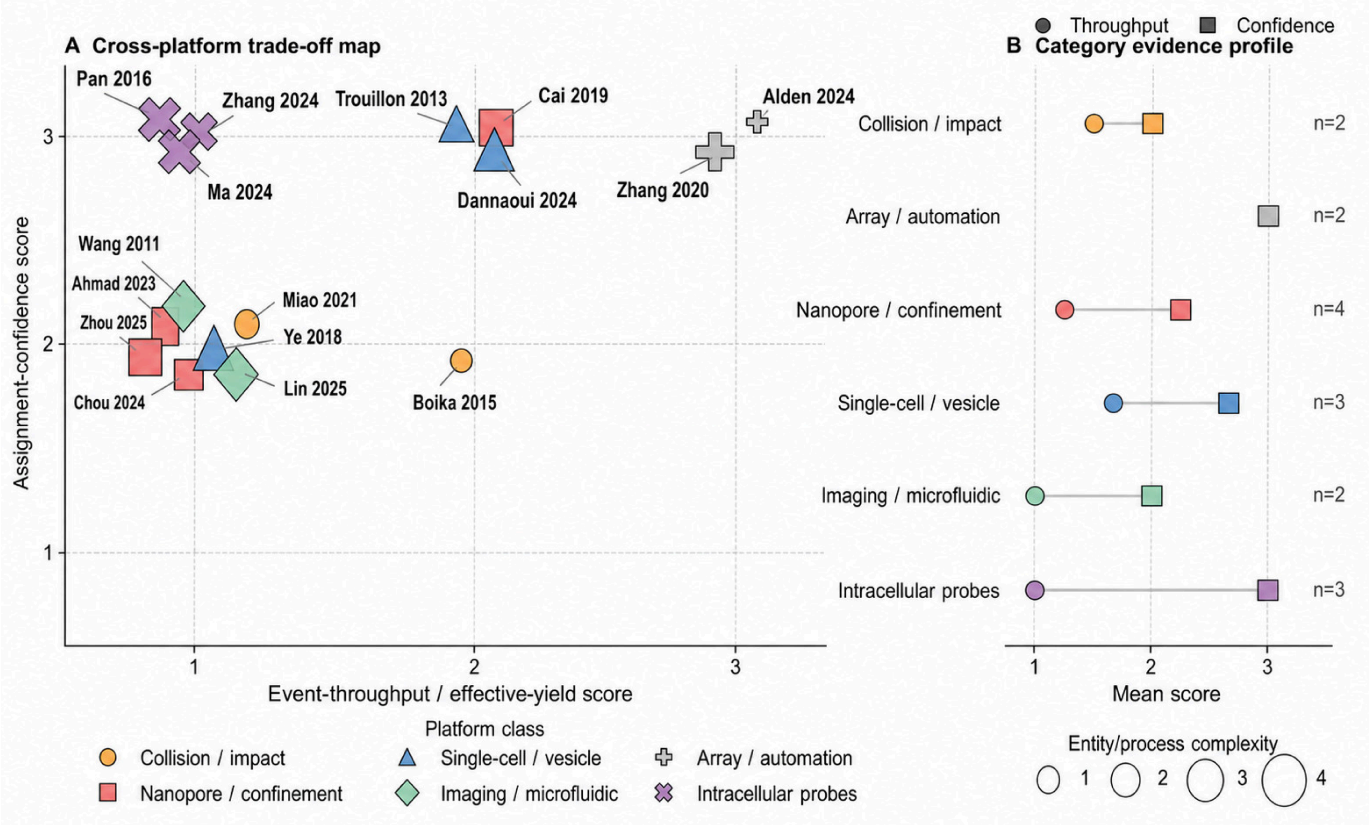


Figure 9. Cross-platform trade-off map of representative SEE strategies. (**A**) Bubble plot showing representative strategies along the ordinal event-throughput/effective-yield score and assignment-confidence score defined in Section 2.3; bubble size indicates the complexity of the assigned entity or process, and color denotes platform class. (**B**) Category-level evidence profile comparing the mean event-throughput/effective-yield and assignment-confidence scores for each platform class. The plot synthesizes the values and evidence bases summarized in Tables 1–3 rather than presenting an independent meta-analysis. The row-level scores, evidence bases, category means, and sensitivity flags are reported in Supplementary Table S1. Data from [2–9,11–13,64,66–68,70].

Recent primary papers make that asymmetry even clearer. A catalase single-entity protein assay can claim pM-range linearity and hundreds of analyzable spikes [86], but that does not make it directly comparable to a bacterial-counting platform whose value lies in label-free cell enumeration and metabolic discrimination [117]. Likewise, a ROS nanocavity electrode with a 1 nM detection limit in a 3D cell model [111] should not be ranked against sub-millisecond semiconductor photoelectrochemistry [54] as if they solved the same problem. The point of cross-platform benchmarking is therefore not to collapse all

formats into one leaderboard, but to make explicit which analytical bottleneck each study actually relieves.

Soft entities and optical-electrochemical single-particle systems sharpen this point further. A nanobubble nanopore sensor may be analytically impressive because it resolves single-digit bubbles and their voltage-dependent transport [51], but that achievement cannot be ranked in the same way as a single-cell nanopipette microviscosity assay reporting about 86 cP in live cancer cells [103]. Nor should single-particle spectroelectrochemistry be collapsed into the same category as classical collision counting merely because both track one entity at a time; in the former, the gain may lie in correlated spectral assignment rather than in lower current limits [59,60]. These examples make the benchmarking problem more difficult, but also more honest.

Sensitivity alone remains the easiest metric to overstate. In molecular nanopore sensing, individual events can be recorded at extremely low analyte abundance, but the analytical meaning of those events depends on how specifically they map to the target. Platforms such as engineered protein nanopores and electro-optical nanopores address this by embedding recognition or orthogonal validation directly into the measurement [2,8]. In high-quality single-cell amperometry, by contrast, the signal-to-noise ratio is often already sufficient; the more important issue is whether spike analysis can distinguish vesicle content, release fraction, and pore dynamics without conflating them [6,70]. Vesicle electrochemical cytometry makes this especially obvious, because oxidation completeness can shift from roughly 75% to nearly 100% depending on whether a vesicle opens at a conical nanotip or a flat disk, and quantitative confidence can increase more by pairing resistive sizing with charge integration than by simply recording more events [90,91]. Thus, the same sensitivity claim can mean very different things depending on whether the bottleneck is event visibility, mechanistic assignment, or biological interpretation.

Temporal resolution offers a similarly mixed picture. Single-cell amperometry remains hard to beat for resolving sub-second secretion kinetics, whereas coupled nanopores and related confined systems are beginning to address a different problem: how to slow or structure microsecond-scale translocations so that information is not lost to bandwidth limits [64]. Sampling rate and filter bandwidth should therefore be distinguished explicitly: sampling rate describes how frequently the current is digitized, whereas filter bandwidth determines the highest-frequency signal component retained for event identification. This comparison reveals an important principle. Temporal resolution is only analytically valuable when it matches the relevant process. More bandwidth is not automatically better if the event remains chemically ambiguous; less bandwidth is not automatically fatal if the platform intentionally reshapes transport to preserve informative features. The most credible studies therefore optimize timing and interpretability together rather than treating them as separate goals.

5.2. Throughput, Standardization, Statistics, and Reproducibility

If the first decade of SEE was dominated by making single events visible, the next decade is likely to be dominated by making large numbers of single events comparable. Throughput has become decisive because single-entity measurements are intrinsically distributional: one does not only want to know that an event can occur, but how frequently, how variably, and under what conditions it shifts across populations of particles, vesicles, or cells. Alden et al. [6] demonstrated the analytical impact of this shift by collecting 3270 nanoparticle-impact events from 671 microelectrodes within a few hours and using automated analysis to extract statistically robust distributions. Zhang et al. [67] similarly showed that array-based chips can merge manipulation and readout at the single-cell

level, moving electrochemical assays toward device-compatible phenotyping rather than artisanal one-cell-at-a-time probing.

These advances explain why machine learning and data infrastructure are no longer optional side topics. The challenge is not simply to classify more events, but to do so without losing the mechanistic grounding that makes SEE analytically credible. Recent work on automated event analysis and field-level data handling suggests that the next bottleneck is standardization of raw data formats, event-labeling logic, and cross-platform reporting conventions [6,122]. Without that layer, two studies may both report thousands of events while remaining difficult to compare because filtering rules, event thresholds, or quality-control procedures differ. Reproducibility in SEE therefore depends as much on transparent data treatment as on electrode fabrication.

The current literature already shows why such reporting standards must go beyond a simple event count. Dannaoui et al. [70] found that only about 84% of a representative spike set was analyzable by their model, with 97 double-exponential spikes and 9 single-exponential spikes in one explicitly discussed data subset. That level of transparency is far more informative than reporting only a few archetypal peaks, because it tells the reader how much of the experiment actually supported the mechanistic inference. Similarly, first-arrival collision analysis used at least 10 replicate measurements at each of 0.145, 1.45, and 14.5 fM rather than presenting a single best-case trace [5]. These examples reveal a broader principle: a strong SEE paper should report the denominator as carefully as the numerator, including the numbers of collected, discarded, and ambiguous events as well as the algorithmic rules used for classification. Without those numbers, reproducibility claims remain incomplete even when individual traces are well resolved.

This point becomes even sharper when different analytical modes are compared side by side. In nanopore sensing, the crucial denominator may capture probability or the fraction of bound states that can be distinguished at a fixed bandwidth. In intracellular single-cell work, it may be the fraction of successful insertions, the percentage of stable baselines after penetration, or the proportion of cells that remain viable after probe manipulation. In array-based work, it may be the number of functional electrodes or the distribution of silent channels across a chip. The reason to insist on these metrics is not bureaucratic completeness. It is that SEE increasingly operates at the boundary where failed or silent events are analytically meaningful. If an interface detects only a small and highly selected subset of entities, the missing events are part of the measurement reality and must be reported as such.

Practical standardization also includes what is often omitted from headline figures: probe placement reproducibility, sample handling, fouling control, and the rate of silent or unusable events. This is especially critical in intracellular and molecular sensing, where the success fraction of measurements can be low even when the reported events are elegant. The field needs a stronger norm of reporting not only the best examples but the effective yield of analyzable events per experiment. Such reporting would make the comparisons in Table 3 far more meaningful and would help distinguish robust analytical workflows from technically impressive but fragile demonstrations.

5.3. Where Electrochemistry Outperforms, Complements, or Lags Behind Adjacent Single-Entity Methods

SEE competes indirectly with several neighboring single-entity methods, including fluorescence imaging, optical single-particle tracking, patch-clamp electrophysiology, nanopore sequencing-style sensing, and increasingly single-cell omics. It rarely wins on all axes at once. Its real advantage lies in the combination of interfacial sensitivity, kinetic fidelity, and direct access to redox or transport processes. When the analytical objective concerns secretion dynamics, catalytic heterogeneity, molecular translocation under bias,

or local physicochemical state, electrochemistry can provide mechanistic and temporal information that optical and omics methods do not naturally deliver [3,10,11]. This is why electrochemical single-cell measurements remain so valuable even in an era dominated by sequencing-based heterogeneity maps.

SEE's advantage is clearest when framed comparatively rather than rhetorically. A chloride nanopipette that reaches a near-Nernstian 56.6 mV per decade response with 120 ms response time offers something different from a fluorescence image of chloride distribution: less structural breadth, but more immediate electrochemical calibration at the local interface [66]. A plasmonic impedance platform with about 2 pS sensitivity and millisecond resolution cannot identify every molecular actor in a cell, but it can track electrically meaningful changes label-free in space and time [4]. A collision array that yields 3270 events from 671 electrodes does not deliver transcriptomic dimensionality, but it does produce experimentally grounded distributions on a timescale and with a directness that many omics pipelines cannot match [6]. Fresh-brain synaptic vesicle electrochemistry offers a different but equally telling comparison: it cannot match the molecular breadth of tissue omics, yet it directly quantifies vesicular monoamine in situ and can be paired with pharmacological perturbation, as shown by oxaliplatin-associated remodeling of vesicular storage and release in fresh brain slices and isolated neurons [96,97]. SEE is therefore strongest when the analytical objective is inherently interfacial, kinetic, or redox specific. When the objective instead demands broad molecular inventory or unambiguous structural assignment, electrochemistry is more likely to play a complementary than leading role.

This comparative advantage is becoming easier to see as the target space broadens. Semiconductor SEE can relate photocurrent transients to local charge transport in ways that purely optical particle tracking cannot [54,55]. Condensate-resolved ROS measurements and low-copy-number intracellular enzyme trapping address subcellular chemical questions that are difficult to reach with ensemble omics [110,112]. Bacterial SEE, meanwhile, offers a fast route to functional counting and phenotype-linked electrochemical discrimination without labels or sequencing [117,118]. These examples do not erase the limits of electrochemistry, but they do sharpen where it is most distinctive: whenever interfacial flux, redox turnover, or localized chemical dynamics are the quantity of interest.

The same is true for several newer branches that might otherwise look peripheral. Nanodroplet and nanoemulsion studies provide direct access to liquid–liquid interfacial kinetics and event-by-event partitioning behavior that are difficult to reconstruct from bulk electrochemical measurements [33,49]. Single-particle spectroelectrochemistry of Au nanorods offers a route to correlate activity, ligand-state damping, and plasmonic response on one catalyst instead of inferring those relations from separate optical and electrochemical ensembles [59–61]. Single-molecule RNA-degradation sensing, in turn, suggests that nanopore electroanalysis can contribute to biomolecular quality control as well as yes-no target recognition [75]. These directions do not reduce the field's fragmentation, but they clarify where electrochemistry offers uniquely local, kinetic, or interfacial information even when adjacent methods provide broader compositional coverage.

Where SEE lags is equally important. Molecular breadth is narrow relative to omics, absolute structural assignment is weaker than in high-end single-molecule fluorescence or mass spectrometry, and experimental standardization remains less mature than in established bioanalytical platforms. In addition, many SEE experiments still depend on custom-fabricated probes, specialized interpretation, or narrow analyte classes. These are not fatal limitations, but they define the conditions under which electrochemistry should be deployed strategically rather than aspirationally.

There is also a more subtle limitation that becomes visible only when one compares across subfields. In exocytosis and some collision measurements, electrochemical signals

are already closely aligned with the measured process: charge can be related to molecule number, current steps can be related to catalytic arrival, and event rates can often be linked to concentration or transport. In many molecular-recognition nanopore studies, by contrast, the electrochemical signal is only one layer in a longer inferential chain involving pore occupancy, conformational state, binding-site geometry, and model-based classification. Those systems may still be analytically powerful, but they demand a different standard of validation than a classical amperometric spike. Progress in SEE will be slowed if these epistemic differences are ignored. It will be accelerated if the field becomes more explicit about which classes of claim are direct, which are model dependent, and which require orthogonal confirmation.

The most promising future therefore lies in complementarity. Transparent electrodes, photoelectrochemical coupling, electro-optical nanopores, and probe designs that combine localized perturbation with real-time readout all point toward hybrid measurement ecosystems rather than isolated electrochemical devices [2,10–12]. Figure 10 brings these hybrid workflows together, showing that the strongest application-facing future of SEE will likely emerge when electrochemistry supplies the fast, local, interfacial readout within a multimodal workflow that adds orthogonal specificity or higher-level biological context.

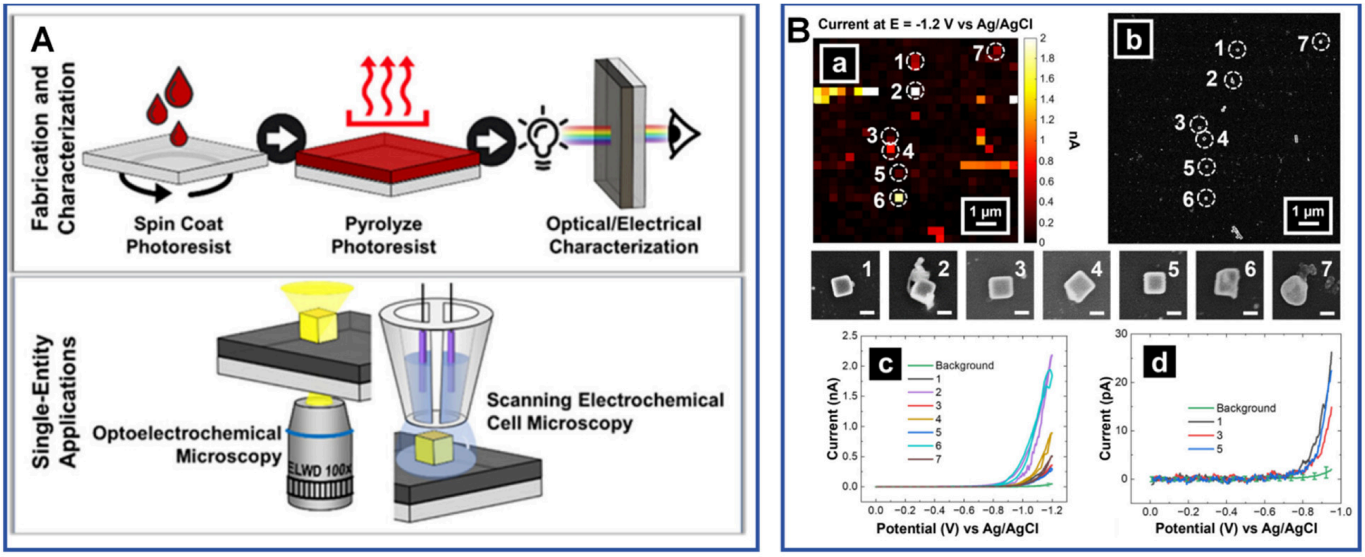


Figure 10. (**A**) Schematic of OTCE fabrication process and OTCEs in-use for SEE. (**Ba**) SECCM voltammetric map and (**Bb**) correlated SEM image of the SECCM scan area for Au NCs on an OTCE. (**Bc**) CVs of HER on seven individual nanoparticles from scan where the number for each trace color relates to the SEM images of the individual nanoparticles directly above the CV plots (scale bar: 100 nm). (**Bd**) LSVs of NCs 1, 3, and 5 extrapolated from data shown in (**Bc**). Adapted from [123] under the terms of the Creative Commons Attribution License.

6. Challenges and Future Perspectives

6.1. Instrumental and Interfacial Bottlenecks

The most persistent bottleneck in SEE remains the interface itself. At ultimate sensitivity, the electrode or pore is no longer a neutral observer; it shapes the event through surface charge, adsorption, fouling, local electric field, and geometry-dependent transport. This is true for nanoparticle impacts, nanopore sensing, single-cell amperometry, and intracellular probing alike. The problem is not simply that surfaces age or drift, but that interfacial variation can masquerade as entity heterogeneity. A change in blockade distribution may reflect altered analyte populations, or it may reflect altered pore chemistry. A difference in amperometric spike width may reflect changed fusion dynamics, or it may arise from

modified cell-surface architecture or electrode condition [3,64]. The closer the field moves toward one-molecule and one-cell limits, the more this ambiguity becomes central rather than peripheral.

Instrumental noise is only one part of this challenge. Capacitance, filtering, amplifier bandwidth, and mechanical stability still matter, especially in fast molecular translocation experiments, but surface reproducibility and event yield are increasingly limiting. For single-cell intracellular analysis, the probe must be small enough to localize chemistry without irreversibly perturbing the cell, yet robust enough to survive insertion and calibration [9,65,66]. For nanopore sensing, pore-to-pore reproducibility and capture efficiency remain major constraints on interlaboratory transfer [8,64]. A key future direction is therefore not merely fabricating smaller interfaces, but fabricating interfaces whose behavior is more predictable and more reportable across studies.

The quantitative comparisons in Tables 1–3 make this challenge visible across otherwise unrelated platforms. Chou et al. [64] deliberately engineered a top sensing pore of about 2 nm and varied the number of lower guiding pores from 1 to 9 to reshape transport rather than simply to shrink the detector. Zhou et al. [13] used 12 $\pm$ 2 nm membranes with 8.64 and 8.84 nm pores and collected data at 100 kHz with 10 kHz low-pass filtering, showing that even ostensibly straightforward protein sensing depends on tightly specified geometry and bandwidth. In intracellular work, the trade-off is different but no less severe: the chloride nanopipette gained analytical credibility by explicitly pairing a 500 nm aperture with a calibrated Nernstian response, while the ROS/temperature nanoprobe accepted a larger insulated footprint to obtain dual calibration ranges [9,66]. What these examples share is that geometry is not background information. It is a first-order analytical variable that controls whether an event is visible, interpretable, and comparable.

This is also why the field should resist the temptation to describe every new platform as merely "minimally invasive" or "highly sensitive" without quantitative context. A probe with a slightly larger diameter may in practice be analytically superior if it yields a reproducible current baseline, a stable insertion protocol, and a defensible calibration model. Likewise, a nanopore with more structured transport may outperform a nominally smaller pore if its events are easier to assign and less vulnerable to pore-to-pore variation. The most useful future instrumental papers will therefore not only introduce new interfaces, but will report how those interfaces distribute performance across repeated pores, electrodes, or cells. In other words, the next frontier in interface engineering is not just smaller dimensions, but tighter distributions.

Enabling fabrication papers deserve more credit here than they usually receive. Reproducible nanopipette-based electroplated nanoelectrodes with controllable RG and metal composition do not by themselves solve a biological problem, but they directly reduce one of the biggest hidden sources of single-entity variability: uncontrolled interface geometry [108]. In the same spirit, in vivo ion-selective micropipette sensors remind us that interface robustness must eventually survive real tissue environments rather than only buffered calibration cells [107]. For a mature analytical field, such fabrication and deployment studies are not peripheral. They define whether more complex biological demonstrations can be repeated elsewhere.

6.2. Standardization, Multimodal Coupling, and Data Science Opportunities

The next bottleneck is informational. SEE now generates data that are richer and more heterogeneous than the field's reporting conventions were designed to handle. Event traces are often filtered, segmented, thresholded, and classified through custom pipelines, yet many manuscripts still provide only summary plots rather than the logic by which raw events became analytical conclusions. Recent work on field development and machine

learning argues persuasively that SEE needs common expectations for event annotation, negative controls, metadata capture, and data sharing if cross-platform benchmarking is to become meaningful [6,122]. Without this, even genuine progress remains difficult to compare.

Multimodal coupling is likely to solve part of this problem by making assignment more robust. Electro-optical nanopores, bipolar electrochemiluminescence nanoprobes, photoelectrochemical single-particle platforms, and perturb-and-measure microfluidic probes all share the same analytical philosophy: use electrochemistry for local, high-time-resolution readout, but pair it with an orthogonal channel that increases specificity or biological context [2,10–12]. This trend should not be seen as a departure from electrochemistry. Rather, it is evidence that electrochemistry is becoming the high-bandwidth interfacial core of broader single-entity analytical systems.

For analytical chemistry, the key opportunity is to turn that multimodality into standardized evidential logic rather than into ad hoc visual confirmation. Cai et al. [2] did not merely add fluorescence to make the experiment look richer; they used synchronized optical and electrical events to support pM-level affinity and detection-limit claims that would otherwise have remained model dependent. Wang et al. [10] similarly used nanopipette-confined bipolar electrochemiluminescence to translate intracellular chemistry into an optical output while spatially restricting the applied potential inside the pipette. The common lesson is that orthogonal channels are most valuable when they resolve specific ambiguities in the electrochemical readout, including binding validity, probe localization, and discrimination between target reactions and parasitic interfacial processes. Future multimodal SEE should therefore be judged not by how many channels are added, but by whether each additional channel reduces a defined uncertainty in assignment or calibration.

Newer single-cell studies show the same logic in a more application-facing form. Au single atom modified carbon nanopipettes paired electrochemical dopamine detection with aptamer-based surface plasmon resonance, producing a multimodal exocytosis workflow that could bridge single-cell and multicell readout while improving electrochemical sensitivity to about 0.049 uM [124]. The analytical value of this kind of design is not that it stacks techniques for decoration, but that it makes cross-validation part of the measurement architecture from the start.

Machine learning will be useful only if deployed within this experimentally grounded framework. Pattern recognition can help classify complex event families, flag outliers, and stabilize throughput at array scale, but it cannot replace mechanistic reasoning. The field will benefit most from models that are linked to explicit hypotheses about event origin, transport, or interfacial dynamics rather than opaque post hoc classification. In practical terms, the best future SEE studies will likely combine mechanistic controls, structured metadata, and data-driven event analysis rather than treating these as separate layers. This view is consistent with two recent field-level reviews, which emphasize both rapid methodological diversification in SEE and the need to compare single-entity electrocatalysis by mechanism, data treatment, and deployment readiness rather than by nominal sensitivity alone [125,126].

6.3. Roadmap to Robust Single-Molecule and Single-Cell Electroanalysis

The route from compelling demonstrations to robust analytical workflows can be framed around four priorities. First, assignment confidence must become a reportable performance metric alongside sensitivity and time resolution. This means explicitly quantifying silent events, nonspecific events, and classification uncertainty. Second, throughput must increase without sacrificing mechanistic clarity; arrays, multiplexed nanopores, and automated probes are therefore as important as lower-noise amplifiers. Third, multimodal validation should be embraced where it materially improves specificity. Fourth,

the field should standardize around application domains where electrochemistry has a clear comparative advantage, such as secretion dynamics, catalytic heterogeneity, redox microenvironments, and localized perturbation-response analysis.

A practical extension of this roadmap is to define a minimum reporting bundle for entity-resolved electrochemical papers. For molecular and nanopore studies, that bundle should include pore or electrode geometry, sampling rate, filter setting, capture or event yield, number of rejected events, and the calibration target used to translate event statistics into an analytical claim. For single-cell and intracellular studies, it should further include probe dimensions after insulation, insertion success fraction, cell viability after manipulation, response time, calibration range, and the number of cells, vesicles, or synapses contributing to the reported distributions. Several of the strongest papers reviewed here already move in this direction: 84% analyzable spikes were reported explicitly in one mechanistic exocytosis study, a 4 × 4 array architecture was paired with viability and recovery metrics in a single-cell device paper, and intracellular glucose analysis reported local delivery volume, calibration window, and inferred cellular concentration rather than only a representative trace [67,68,70]. The point is not to force every experiment into one template, but to ensure that future cross-study benchmarking rests on more than the best-looking events.

If such reporting norms become standard, the field's next decade could look very different from its first. Reviews would be able to compare not only whether a signal was observed, but under what success rate, with what uncertainty, and after what degree of data curation. Machine learning models could be trained on richer, better annotated event libraries. Multimodal designs could be evaluated by how much ambiguity they actually remove. Most importantly, the ultimate goals named in this review, detecting single molecules and interrogating single cells, would no longer be endpoints defined mainly by isolated proof-of-concept demonstrations. They would become operational analytical categories with recognizable standards of evidence.

Figure 11 synthesizes this roadmap. It places materials and interface engineering, event-confidence modeling, multimodal validation, and standardized benchmarking on one axis, and maps them onto the two analytical endpoints emphasized throughout this review: trustworthy single-molecule detection and context-preserving single-cell analysis. The message is deliberately realistic. SEE is unlikely to converge on a single universal platform. Instead, it will mature as a family of electrochemically controlled, data-rich, entity-resolved measurement strategies whose analytical credibility depends on how well they integrate interface design, statistics, and application-specific validation.

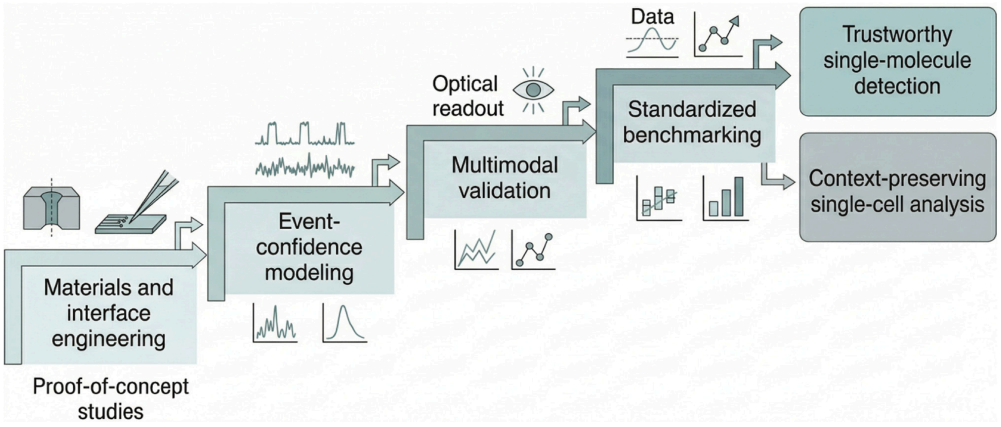


Figure 11. Future-outlook roadmap for advancing SEE from proof-of-concept demonstrations to robust analytical workflows.

7. Conclusions

SEE has progressed from observing isolated stochastic events to building analyte- and context-specific frameworks for interpreting them. The strongest body of evidence currently lies in single-cell amperometry and related secretion studies, where event statistics, mechanistic models, and biologically meaningful heterogeneity are tightly coupled. The main frontier in single-molecule analysis lies in nanopores, nanoconfinement, and multimodal validation, where rare-event readout is being converted into increasingly reliable molecular information. Across both areas, however, the decisive issue is no longer whether one entity can in principle be detected, but whether entity-resolved measurements can be assigned, quantified, compared, and reproduced with the rigor expected of analytical chemistry. Progress toward the stated analytical limits will depend on treating sensitivity as one performance dimension rather than the sole endpoint, and on optimizing confidence of assignment, throughput, interfacial reproducibility, and application relevance in parallel. Under that criterion, SEE has progressed well beyond a specialized niche, but it is not yet uniformly mature. Its future analytical impact will depend on converting well-resolved events into standardized, evidence-rich workflows for detecting single molecules and interrogating single cells.

The current literature supports this conclusion, but with important limits. The field now possesses several ingredients needed for broader analytical maturity: event-resolved hardware, sub-second and even microsecond measurements, pM-level affinity readouts, calibrated intracellular probes, array-scale acquisition, and the first generation of data-centric analysis frameworks. What it still lacks is uniformity of evidential practice. Some studies already report cell counts, event counts, calibration ranges, and filtering conditions in a way that supports real cross-study comparison; others still rely too heavily on exemplary traces and qualitative claims of sensitivity. Accordingly, rigorous development of SEE will depend on quantitative discipline, explicit denominators, transparent modeling, traceable figure and table sourcing, and a reporting culture that values comparability as much as novelty.

Supplementary Materials: The following supporting information can be downloaded at: https://www.mdpi.com/article/10.3390/chemosensors14070153/s1, Supplementary Table S1 (row-level score assignments, evidence bases, category means, and sensitivity flags for Figure 9) is provided as a separate file.

Author Contributions: L.F. contributed to conceptualization, methodology, supervision, project administration, and writing—review and editing. F.C. contributed to investigation, data curation, formal analysis, and writing—original draft. Y.L. contributed to literature collection, data curation, visualization, and formal analysis. S.Z. contributed to investigation, validation, and writing—review and editing. C.-T.L. contributed to supervision, resources, validation, and writing—review and editing. All authors have read and agreed to the published version of the manuscript.

Funding: This research received no external funding.

Institutional Review Board Statement: Not applicable.

Informed Consent Statement: Not applicable.

Data Availability Statement: No new data were created or analyzed in this study.

Conflicts of Interest: The authors declare no conflicts of interest.

References

1. Xiao, X.; Bard, A.J. Observing Single Nanoparticle Collisions at an Ultramicroelectrode by Electrocatalytic Amplification. *J. Am. Chem. Soc.* **2007**, *129*, 9610–9612. [CrossRef] [PubMed]
2. Cai, S.; Sze, J.Y.Y.; Ivanov, A.P.; Edel, J.B. Small Molecule Electro-Optical Binding Assay Using Nanopores. *Nat. Commun.* **2019**, *10*, 1797. [CrossRef] [PubMed]

3. Trouillon, R.; Ewing, A.G. Single Cell Amperometry Reveals Glycocalyx Hinders the Release of Neurotransmitters During Exocytosis. *Anal. Chem.* **2013**, *85*, 4822–4828. [CrossRef] [PubMed]
4. Wang, W.; Foley, K.; Shan, X.; Wang, S.; Eaton, S.; Nagaraj, V.J.; Wiktor, P.; Patel, U.; Tao, N. Single Cells and Intracellular Processes Studied by a Plasmonic-Based Electrochemical Impedance Microscopy. *Nat. Chem.* **2011**, *3*, 249–255. [CrossRef] [PubMed]
5. Boika, A.; Bard, A.J. Time of First Arrival in Electrochemical Collision Experiments as a Measure of Ultralow Concentrations of Analytes in Solution. *Anal. Chem.* **2015**, *87*, 4341–4346. [CrossRef] [PubMed]
6. Alden, S.E.; Zhang, L.; Wang, Y.; Lavrik, N.V.; Thorgaard, S.N.; Baker, L.A. High-Throughput Single-Entity Electrochemistry with Microelectrode Arrays. *Anal. Chem.* **2024**, *96*, 9177–9184. [CrossRef] [PubMed]
7. Ye, D.; Gu, C.; Ewing, A. Using Single-Cell Amperometry and Intracellular Vesicle Impact Electrochemical Cytometry to Shed Light on the Biphasic Effects of Lidocaine on Exocytosis. *ACS Chem. Neurosci.* **2018**, *9*, 2941–2947. [CrossRef] [PubMed]
8. Ahmad, M.; Ha, J.-H.; Mayse, L.A.; Presti, M.F.; Wolfe, A.J.; Moody, K.J.; Loh, S.N.; Movileanu, L. A Generalizable Nanopore Sensor for Highly Specific Protein Detection at Single-Molecule Precision. *Nat. Commun.* **2023**, *14*, 1374. [CrossRef] [PubMed]
9. Ma, Y.; Hu, W.; Hu, J.; Ruan, M.; Hu, J.; Yang, M.; Zhang, Y.; Xie, H.; Hu, C. Bifunctional Nanoprobe for Simultaneous Detection of Intracellular Reactive Oxygen Species and Temperature in Single Cells. *Microsyst. Nanoeng.* **2024**, *10*, 171. [CrossRef] [PubMed]
10. Wang, Y.; Jin, R.; Sojic, N.; Jiang, D.; Chen, H. Intracellular Wireless Analysis of Single Cells by Bipolar Electrochemiluminescence Confined in a Nanopipette. *Angew. Chem. Int. Ed.* **2020**, *59*, 10416–10420. [CrossRef] [PubMed]
11. Miao, R.; Shao, L.; Compton, R.G. Single Entity Electrochemistry and the Electron Transfer Kinetics of Hydrazine Oxidation. *Nano Res.* **2021**, *14*, 4132–4139. [CrossRef]
12. Lin, J.; Hou, Y.; Wu, Z.; Song, Y.; Zhang, Q.; Lin, J. Single-Cell Localized Treatment and ROS Dynamics Monitoring via an Open Electrochemical-Microfluidic Probe. *Small* **2025**, *21*, 2503911. [CrossRef] [PubMed]
13. Zhou, Z.-Q.; Liu, S.-C.; Wang, J.; Chen, K.-L.; Xie, B.-K.; Ying, Y.-L.; Long, Y.-T. Exploring a Solid-State Nanopore Approach for Single-Molecule Protein Detection from Single Cells. *Chem. Sci.* **2025**, *16*, 8501–8508. [CrossRef] [PubMed]
14. Quinn, B.M.; Van'T Hof, P.G.; Lemay, S.G. Time-Resolved Electrochemical Detection of Discrete Adsorption Events. *J. Am. Chem. Soc.* **2004**, *126*, 8360–8361. [CrossRef] [PubMed]
15. Kwon, S.J.; Fan, F.-R.F.; Bard, A.J. Observing Iridium Oxide (IrO_x) Single Nanoparticle Collisions at Ultramicroelectrodes. *J. Am. Chem. Soc.* **2010**, *132*, 13165–13167. [CrossRef] [PubMed]
16. Bai, Y. Single-Nanoparticle Electrochemical Collision for Monitoring Self-Assembly of Thiol Molecules on Au Nanoparticles. *Biosensors* **2024**, *14*, 393. [CrossRef] [PubMed]
17. Sundar, S.; Kim, K.J.; Kwon, S.J. Observation of Single Nanoparticle Collisions with Green Synthesized Pt, Au, and Ag Nanoparticles Using Electrocatalytic Signal Amplification Method. *Nanomaterials* **2019**, *9*, 1695. [CrossRef] [PubMed]
18. Kwon, S.J.; Bard, A.J. Analysis of Diffusion-Controlled Stochastic Events of Iridium Oxide Single Nanoparticle Collisions by Scanning Electrochemical Microscopy. *J. Am. Chem. Soc.* **2012**, *134*, 7102–7108. [CrossRef] [PubMed]
19. Kim, J.; Kim, B.-K.; Cho, S.K.; Bard, A.J. Tunneling Ultramicroelectrode: Nanoelectrodes and Nanoparticle Collisions. *J. Am. Chem. Soc.* **2014**, *136*, 8173–8176. [CrossRef] [PubMed]
20. Ganguli, S.; Zhao, Z.; Parlak, O.; Hattori, Y.; Sá, J.; Sekretareva, A. Nano-Impact Single-Entity Electrochemistry Enables Plasmon-Enhanced Electrocatalysis. *Angew. Chem. Int. Ed.* **2023**, *62*, e202302394. [CrossRef] [PubMed]
21. Liu, Z.; Amin, H.M.A.; Peng, Y.; Corva, M.; Pentcheva, R.; Tschulik, K. Facet-Dependent Intrinsic Activity of Single Co_3O_4 Nanoparticles for Oxygen Evolution Reaction. *Adv. Funct. Mater.* **2023**, *33*, 2210945. [CrossRef]
22. Xiao, X.; Fan, F.-R.F.; Zhou, J.; Bard, A.J. Current Transients in Single Nanoparticle Collision Events. *J. Am. Chem. Soc.* **2008**, *130*, 16669–16677. [CrossRef] [PubMed]
23. Xiao, X.; Pan, S.; Jang, J.S.; Fan, F.-R.F.; Bard, A.J. Single Nanoparticle Electrocatalysis: Effect of Monolayers on Particle and Electrode on Electron Transfer. *J. Phys. Chem. C* **2009**, *113*, 14978–14982. [CrossRef]
24. Park, J.H.; Boika, A.; Park, H.S.; Lee, H.C.; Bard, A.J. Single Collision Events of Conductive Nanoparticles Driven by Migration. *J. Phys. Chem. C* **2013**, *117*, 6651–6657. [CrossRef]
25. Rees, N.V.; Zhou, Y.-G.; Compton, R.G. The Non-Destructive Sizing of Nanoparticles via Particle–Electrode Collisions: Tag-Redox Coulometry (TRC). *Chem. Phys. Lett.* **2012**, *525–526*, 69–71. [CrossRef]
26. Chang, X.; Batchelor-McAuley, C.; Compton, R.G. Methanol Oxidation at Single Platinum Nanoparticles. *J. Electroanal. Chem.* **2021**, *896*, 115438. [CrossRef]
27. Lin, J.; Zhao, W.; Li, S.; Wang, J.; Zhang, D.; Zang, Y.; Xin, Q. Electrocatalytic Performance of Single Nanoparticles for Methanol Oxidation Reaction. *J. Electroanal. Chem.* **2023**, *928*, 117045. [CrossRef]
28. Han, L.; Wang, W.; Nsabimana, J.; Yan, J.-W.; Ren, B.; Zhan, D. Single Molecular Catalysis of a Redox Enzyme on Nanoelectrodes. *Faraday Discuss.* **2016**, *193*, 133–139. [CrossRef] [PubMed]
29. Kim, B.-K.; Boika, A.; Kim, J.; Dick, J.E.; Bard, A.J. Characterizing Emulsions by Observation of Single Droplet Collisions—Attoliter Electrochemical Reactors. *J. Am. Chem. Soc.* **2014**, *136*, 4849–4852. [CrossRef] [PubMed]

30. Cheng, W.; Compton, R.G. Quantifying the Electrocatalytic Turnover of Vitamin B_{12}-Mediated Dehalogenation on Single Soft Nanoparticles. *Angew. Chem. Int. Ed.* **2016**, *55*, 2545–2549. [CrossRef] [PubMed]
31. Kim, B.-K.; Kim, J.; Bard, A.J. Electrochemistry of a Single Attoliter Emulsion Droplet in Collisions. *J. Am. Chem. Soc.* **2015**, *137*, 2343–2349. [CrossRef] [PubMed]
32. Madawala, H.; Sabaragamuwe, S.G.; Elangovan, S.; Kim, J. In Situ Measuring Partition Coefficient at Intact Nanoemulsions: A New Application of Single-Entity Electrochemistry. *Anal. Chem.* **2021**, *93*, 1154–1160. [CrossRef] [PubMed]
33. Moon, H.; Park, J.H. In Situ Probing Liquid/Liquid Interfacial Kinetics through Single Nanodroplet Electrochemistry. *Anal. Chem.* **2021**, *93*, 16915–16921. [CrossRef] [PubMed]
34. Reyes-Morales, J.; Moazeb, M.; Colón-Quintana, G.S.; Dick, J.E. The Electrodeposition of Gold Nanoparticles from Aqueous Nanodroplets. *Chem. Commun.* **2022**, *58*, 10663–10666. [CrossRef] [PubMed]
35. Nguyen, T.H.T.; Lee, M.W.; Hong, S.; Ahn, H.S.; Kim, B.-K. Electrosynthesis of Palladium Nanocatalysts Using Single Droplet Reactors and Catalytic Activity for Formic Acid Oxidation. *Electrochim. Acta* **2022**, *401*, 139446. [CrossRef]
36. Reyes-Morales, J.; Vanderkwaak, B.T.; Dick, J.E. Enabling Practical Nanoparticle Electrodeposition from Aqueous Nanodroplets. *Nanoscale* **2022**, *14*, 2750–2757. [CrossRef] [PubMed]
37. Deng, H.; Dick, J.E.; Kummer, S.; Kragl, U.; Strauss, S.H.; Bard, A.J. Probing Ion Transfer across Liquid–Liquid Interfaces by Monitoring Collisions of Single Femtoliter Oil Droplets on Ultramicroelectrodes. *Anal. Chem.* **2016**, *88*, 7754–7761. [CrossRef] [PubMed]
38. Zhang, H.; Sepunaru, L.; Sokolov, S.V.; Laborda, E.; Batchelor-McAuley, C.; Compton, R.G. Electrochemistry of Single Droplets of Inverse (Water-in-Oil) Emulsions. *Phys. Chem. Chem. Phys.* **2017**, *19*, 15662–15666. [CrossRef] [PubMed]
39. Jeun, Y.E.; Baek, B.; Lee, M.W.; Ahn, H.S. Surfactant-Free Electrochemical Synthesis of Metallic Nanoparticles via Stochastic Collisions of Aqueous Nanodroplet Reactors. *Chem. Commun.* **2018**, *54*, 10052–10055. [CrossRef] [PubMed]
40. Pendergast, A.D.; Glasscott, M.W.; Renault, C.; Dick, J.E. One-Step Electrodeposition of Ligand-Free PdPt Alloy Nanoparticles from Water Droplets: Controlling Size, Coverage, and Elemental Stoichiometry. *Electrochem. Commun.* **2019**, *98*, 1–5. [CrossRef]
41. Sabaragamuwe, S.G.; Conti, D.; Puri, S.R.; Andreu, I.; Kim, J. Single-Entity Electrochemistry of Nanoemulsion: The Nanostructural Effect on Its Electrochemical Behavior. *Anal. Chem.* **2019**, *91*, 9599–9607. [CrossRef] [PubMed]
42. Yang, H.; Kwon, H.; Kim, B.-K.; Park, J.H. Electrochemical Detection of Single Attoliter Aqueous Droplets in Electrolyte-Free Organic Solvent via Collision Events. *Electrochim. Acta* **2019**, *320*, 134620. [CrossRef]
43. Park, H.; Park, J.H. In Situ Monitoring of Collision and Recollision Events of Single Attoliter Droplets via Single-Entity Electrochemistry. *J. Phys. Chem. Lett.* **2020**, *11*, 10250–10255. [CrossRef] [PubMed]
44. Sabaragamuwe, S.G.; Madawala, H.; Puri, S.R.; Kim, J. Towards Ultralow Detection Limits of Aromatic Toxicants in Water Using Pluronic Nanoemulsions and Single-Entity Electrochemistry. *Anal. Chim. Acta* **2020**, *1139*, 129–137. [CrossRef] [PubMed]
45. Liu, X.; Chen, X.; Zhang, L.; Twum, K.J.; Wang, X.; Xu, Y.; Zeng, X. Crystalline Silica Particle Functionalized by PEG for Its Collision-Enhanced Detection at Ultramicroelectrode. *Anal. Chim. Acta* **2023**, *1260*, 341178. [CrossRef] [PubMed]
46. Park, J.H.; Ahn, H.S. Electrochemical Synthesis of Multimetallic Nanoparticles and Their Application in Alkaline Oxygen Reduction Catalysis. *Appl. Surf. Sci.* **2020**, *504*, 144517. [CrossRef]
47. Kahk, J.M.; Rees, N.V.; Pillay, J.; Tshikhudo, R.; Vilakazi, S.; Compton, R.G. Electron Transfer Kinetics at Single Nanoparticles. *Nano Today* **2012**, *7*, 174–179. [CrossRef]
48. Vannoy, K.J.; Renault, C.; Dick, J.E. The Microelectrode Insulator Influences Water Nanodroplet Collisions. *Anal. Chem.* **2023**, *95*, 7286–7293. [CrossRef] [PubMed]
49. Du, M.; Zhang, L.; Meng, Y.; Chen, J.; Liu, F. Impact of Surface Chemistry on Emulsion–Electrode Interactions and Electron-Transfer Kinetics in the Single-Entity Electrochemistry. *Anal. Chem.* **2024**, *96*, 1038–1045. [CrossRef] [PubMed]
50. Suvira, M.; Ahuja, A.; Lovre, P.; Singh, M.; Draher, G.W.; Zhang, B. Imaging Single H2 Nanobubbles Using Off-Axis Dark-Field Microscopy. *Anal. Chem.* **2023**, *95*, 15893–15899. [CrossRef] [PubMed]
51. Liu, W.; Zheng, F.; Ma, C.; Xu, W.; Chen, Y.; Sha, J. Single-Digit Nanobubble Sensing via Nanopore Technology. *Anal. Chem.* **2024**, *96*, 9544–9550. [CrossRef] [PubMed]
52. Ha, L.D.; Park, H.; Dinh, T.D.; Park, J.H.; Hwang, S. Disruption Dynamics and Charge Transfer of a Single Attoliter Emulsion Droplet Revealed by Combined Fast-Scan Sinusoidal Voltammetry and Short Time Fourier Transform Analysis. *Anal. Chem.* **2024**, *96*, 18150–18160. [CrossRef] [PubMed]
53. Kim, P.; Moon, H.; Lee, H.C.; Park, J.H. Electrochemical Detection of Single Aqueous Droplets in Organic Solvents via Pitting Collisions. *Anal. Chem.* **2024**, *96*, 4528–4534. [CrossRef] [PubMed]
54. Peng, Y.; Ma, H.; Ma, W.; Long, Y.; Tian, H. Single-Nanoparticle Photoelectrochemistry at a Nanoparticulate TiO_2-Filmed Ultramicroelectrode. *Angew. Chem. Int. Ed.* **2018**, *57*, 3758–3762. [CrossRef] [PubMed]
55. Ahn, H.S.; Bard, A.J. Single-Nanoparticle Collision Events: Tunneling Electron Transfer on a Titanium Dioxide Passivated n-Silicon Electrode. *Angew. Chem. Int. Ed.* **2015**, *54*, 13753–13757. [CrossRef] [PubMed]

56. Huang, K.; Shin, K.; Henkelman, G.; Crooks, R.M. Correlating Surface Structures and Electrochemical Activity Using Shape-Controlled Single-Pt Nanoparticles. *ACS Nano* **2021**, *15*, 17926–17937. [CrossRef] [PubMed]
57. Brasiliense, V.; Clausmeyer, J.; Berto, P.; Tessier, G.; Combellas, C.; Schuhmann, W.; Kanoufi, F. Monitoring Cobalt-Oxide Single Particle Electrochemistry with Subdiffraction Accuracy. *Anal. Chem.* **2018**, *90*, 7341–7348. [CrossRef] [PubMed]
58. Quast, T.; Aiyappa, H.B.; Saddeler, S.; Wilde, P.; Chen, Y.; Schulz, S.; Schuhmann, W. Single-Entity Electrocatalysis of Individual "Picked-and-Dropped" Co_3O_4 Nanoparticles on the Tip of a Carbon Nanoelectrode. *Angew. Chem. Int. Ed.* **2021**, *60*, 3576–3580. [CrossRef] [PubMed]
59. Ramasamy, M.; Ha, J.W. Single-Particle Spectroelectrochemistry: Promoting the Electrocatalytic Activity of Gold Nanorods via Oxygen Plasma Treatment without Structural Deformation. *Anal. Chem.* **2024**, *96*, 737–745. [CrossRef] [PubMed]
60. Ramasamy, M.; Ha, J.W. Single-Particle Spectroelectrochemistry: Revealing the Electrochemical Tuning Mechanism of Chemical Interface Damping in 1,2-Benzenedithiol-Adsorbed Single Gold Nanorods. *Anal. Chem.* **2024**, *96*, 18043–18051. [CrossRef] [PubMed]
61. Ramasamy, M.; Ha, J.W. Single-Particle Spectroelectrochemistry: Plasmon-Mediated Catalytic Activity Enhancement by Electrochemical Surface Engineering in Individual Gold Nanorods. *JACS Au* **2025**, *5*, 4811–4822. [CrossRef] [PubMed]
62. Ramasamy, M.; Ha, J.W. Single-Particle Spectroelectrochemistry: Electrochemical Approaches for Tuning Chemical Interfaces and Plasmon Damping in Single Gold Nanorods. *J. Phys. Chem. Lett.* **2023**, *14*, 5768–5775. [CrossRef] [PubMed]
63. Jena, B.K.; Percival, S.J.; Zhang, B. Au Disk Nanoelectrode by Electrochemical Deposition in a Nanopore. *Anal. Chem.* **2010**, *82*, 6737–6743. [CrossRef] [PubMed]
64. Chou, Y.-C.; Lin, C.-Y.; Castan, A.; Chen, J.; Keneipp, R.; Yasini, P.; Monos, D.; Drndić, M. Coupled Nanopores for Single-Molecule Detection. *Nat. Nanotechnol.* **2024**, *19*, 1686–1692. [CrossRef] [PubMed]
65. Zhang, X.; Qiu, Q.; Jiang, H.; Zhang, F.; Liu, Y.; Amatore, C.; Huang, W. Real-Time Intracellular Measurements of ROS and RNS in Living Cells with Single Core–Shell Nanowire Electrodes. *Angew. Chem. Int. Ed.* **2017**, *56*, 12997–13000. [CrossRef] [PubMed]
66. Zhang, T.-Y.; Liu, F.-Q.; Li, Z.; Xu, Y.-T.; Zhao, W.-W.; Chen, H.-Y.; Xu, J.-J. A Hollow Ag/AgCl Nanoelectrode for Single-Cell Chloride Detection. *Chem. Commun.* **2024**, *60*, 2373–2376. [CrossRef] [PubMed]
67. Zhang, Z.; Zheng, T.; Zhu, R. Single-Cell Individualized Electroporation with Real-Time Impedance Monitoring Using a Microelectrode Array Chip. *Microsyst. Nanoeng.* **2020**, *6*, 81. [CrossRef] [PubMed]
68. Pan, R.; Xu, M.; Jiang, D.; Burgess, J.D.; Chen, H.-Y. Nanokit for Single-Cell Electrochemical Analyses. *Proc. Natl. Acad. Sci. USA* **2016**, *113*, 11436–11440. [CrossRef] [PubMed]
69. Baker, L.A. Perspective and Prospectus on Single-Entity Electrochemistry. *J. Am. Chem. Soc.* **2018**, *140*, 15549–15559. [CrossRef] [PubMed]
70. Dannaoui, R.; Hu, R.; Hu, L.; Tian, Z.-Q.; Svir, I.; Huang, W.-H.; Amatore, C.; Oleinick, A. Vesicular Neurotransmitters Exocytosis Monitored by Amperometry: Theoretical Quantitative Links between Experimental Current Spikes Shapes and Intravesicular Structures. *Chem. Sci.* **2024**, *15*, 13909–13922. [CrossRef] [PubMed]
71. Fan, F.-R.F.; Bard, A.J. Electrochemical Detection of Single Molecules. *Science* **1995**, *267*, 871–874. [CrossRef] [PubMed]
72. Zhang, J.; Kuznetsov, A.M.; Medvedev, I.G.; Chi, Q.; Albrecht, T.; Jensen, P.S.; Ulstrup, J. Single-Molecule Electron Transfer in Electrochemical Environments. *Chem. Rev.* **2008**, *108*, 2737–2791. [CrossRef] [PubMed]
73. Manrao, E.A.; Derrington, I.M.; Laszlo, A.H.; Langford, K.W.; Hopper, M.K.; Gillgren, N.; Pavlenok, M.; Niederweis, M.; Gundlach, J.H. Reading DNA at Single-Nucleotide Resolution with a Mutant MspA Nanopore and Phi29 DNA Polymerase. *Nat. Biotechnol.* **2012**, *30*, 349–353. [CrossRef] [PubMed]
74. Cui, R.; Wang, Z.; Li, L.; Liu, L.; Li, Z.; Liu, X.; Chen, T.; Rauf, A.; Kang, X.; Guo, Y. Bionic Nanopore Recognition Receptors for Single-Molecule Enantioselectivity Studies of Chiral Drugs. *Anal. Chim. Acta* **2024**, *1318*, 342960. [CrossRef] [PubMed]
75. Earle, M.K.; Alawami, M.; Alexii, R.-E.; Brauburger, S.; Keyser, U.F.; Platnich, C.M. Quantifying RNA Degradation with Single-Molecule Nanopore Sensing. *Anal. Chem.* **2025**, *97*, 23841–23847. [CrossRef] [PubMed]
76. Tang, H.; Wang, H.; Zhao, D.; Cao, M.; Zhu, Y.; Li, Y. Nanopore-Based Single-Entity Electrochemistry for the Label-Free Monitoring of Single-Molecule Glycoprotein–Boronate Affinity Interaction and Its Sensing Application. *Anal. Chem.* **2022**, *94*, 5715–5722. [CrossRef] [PubMed]
77. Rand, A.; Zimny, P.; Nagel, R.; Telang, C.; Mollison, J.; Bruns, A.; Leff, E.; Reisner, W.W.; Dunbar, W.B. Electronic Mapping of a Bacterial Genome with Dual Solid-State Nanopores and Active Single-Molecule Control. *ACS Nano* **2022**, *16*, 5258–5273. [CrossRef] [PubMed]
78. Liu, R.; Wang, D. Pressure-Regulated Single-Entity Electrochemistry Inside Carbon Nanopipettes. *ACS Sens.* **2022**, *7*, 1138–1144. [CrossRef] [PubMed]
79. Cadinu, P.; Campolo, G.; Pud, S.; Yang, W.; Edel, J.B.; Dekker, C.; Ivanov, A.P. Double Barrel Nanopores as a New Tool for Controlling Single-Molecule Transport. *Nano Lett.* **2018**, *18*, 2738–2745. [CrossRef] [PubMed]
80. Wang, C.; Sensale, S.; Pan, Z.; Senapati, S.; Chang, H.-C. Slowing down DNA translocation through solid-state nanopores by edge-field leakage. *Nat. Commun.* **2021**, *12*, 140. [CrossRef] [PubMed]

81. Chen, K.; Jou, I.; Ermann, N.; Muthukumar, M.; Keyser, U.F.; Bell, N.A.W. Dynamics of Driven Polymer Transport through a Nanopore. *Nat. Phys.* **2021**, *17*, 1043–1049. [CrossRef]
82. Chen, K.; Gularek, F.; Liu, B.; Weinhold, E.; Keyser, U.F. Electrical DNA Sequence Mapping Using Oligodeoxynucleotide Labels and Nanopores. *ACS Nano* **2021**, *15*, 2679–2685. [CrossRef] [PubMed]
83. Yang, C.-N.; Liu, W.; Liu, H.-T.; Zhang, J.-C.; Long, Y.-T.; Ying, Y.-L. Electrochemical Kinetic Fingerprinting of Single-Molecule Coordinations in Confined Nanopores. *Faraday Discuss.* **2025**, *257*, 29–43. [CrossRef] [PubMed]
84. Wang, Y.; Qi, B.; Huang, Y. Bilayer-Coupled Nanopores for Tracking and Detecting Single Unmodified Molecules. *Matter* **2024**, *7*, 4137–4138. [CrossRef]
85. Zhao, Z.; Kostopoulos, N.; Ganguli, S.; Bergstrom, P.; Sekretareva, A. Single-Entity Protein Electrochemistry of a Diffusion-Limited Enzyme. *ACS Electrochem.* **2025**, *1*, 1352–1359. [CrossRef]
86. Kwon, S.J.; Bard, A.J. DNA Analysis by Application of Pt Nanoparticle Electrochemical Amplification with Single Label Response. *J. Am. Chem. Soc.* **2012**, *134*, 10777–10779. [CrossRef] [PubMed]
87. Larsson, A.; Majdi, S.; Oleinick, A.; Svir, I.; Dunevall, J.; Amatore, C.; Ewing, A.G. Intracellular Electrochemical Nanomeasurements Reveal That Exocytosis of Molecules at Living Neurons Is Subquantal and Complex. *Angew. Chem. Int. Ed.* **2020**, *59*, 6711–6714. [CrossRef] [PubMed]
88. Dannaoui, R.; Svir, I.; Huang, W.-H.; Amatore, C.; Oleinick, A. Modeling the Detection of Transient Vesicular Exocytotic Release from Single Cells with Cylindrical Enzymatic Nanoelectrodes. *Electrochim. Acta* **2024**, *508*, 145214. [CrossRef]
89. Li, X.; Dunevall, J.; Ren, L.; Ewing, A.G. Mechanistic Aspects of Vesicle Opening during Analysis with Vesicle Impact Electrochemical Cytometry. *Anal. Chem.* **2017**, *89*, 9416–9423. [CrossRef] [PubMed]
90. Li, X.; Ren, L.; Dunevall, J.; Ye, D.; White, H.S.; Edwards, M.A.; Ewing, A.G. Nanopore Opening at Flat and Nanotip Conical Electrodes during Vesicle Impact Electrochemical Cytometry. *ACS Nano* **2018**, *12*, 3010–3019. [CrossRef] [PubMed]
91. Zhang, X.-W.; Hatamie, A.; Ewing, A.G. Simultaneous Quantification of Vesicle Size and Catecholamine Content by Resistive Pulses in Nanopores and Vesicle Impact Electrochemical Cytometry. *J. Am. Chem. Soc.* **2020**, *142*, 4093–4097. [CrossRef] [PubMed]
92. Hatamie, A.; Ren, L.; Zhang, X.; Ewing, A.G. Vesicle Impact Electrochemical Cytometry to Determine Carbon Nanotube-Induced Fusion of Intracellular Vesicles. *Anal. Chem.* **2021**, *93*, 13161–13168. [CrossRef] [PubMed]
93. He, X.; Ewing, A.G. Anionic Species Regulate Chemical Storage in Nanometer Vesicles and Amperometrically Detected Exocytotic Dynamics. *J. Am. Chem. Soc.* **2022**, *144*, 4310–4314. [CrossRef] [PubMed]
94. Cao, L.; Zhang, J.; Li, M.; Zhou, J.; Liu, Y.; Liu, C.; Li, X. Single-Vesicle Electrochemistry Reveals Polysaccharide from *Glochidion eriocarpum* Champ. Regulates Vesicular Storage and Exocytotic Release of Dopamine. *Anal. Chem.* **2024**, *96*, 15248–15256. [CrossRef] [PubMed]
95. Makam, A.A.; Wahlund, J.; Gandasi, N.R.; Hatamie, A. Single-Vesicle Microelectroanalysis Reveals the Role of PIP2 Phospholipid in Vesicle Opening Dynamics and Its Potential Role in Exocytosis. *ACS Omega* **2025**, *10*, 18889–18898. [CrossRef] [PubMed]
96. Liu, Y.; Cao, L.; Zhou, J.; Li, C.; Du, J.; Xue, Y.; Li, X.; Mao, L. Single-Vesicle Electrochemistry in Fresh Brain Slices Enables in Situ Quantification of Vesicular Monoamine. *J. Am. Chem. Soc.* **2025**, *147*, 149–160. [CrossRef] [PubMed]
97. Chen, J.; Liu, Y.; Cao, L.; Zhou, J.; Nan, X.; Li, C.; Liu, W.; Xiong, M.; Jiang, Y.; Dai, Q.; et al. Investigating the Effect of Oxaliplatin on Vesicular Dopamine Cargo and Release Dynamics in Brain with Single-Vesicle Electrochemistry. *Anal. Chem.* **2026**, *98*, 3307–3315. [CrossRef] [PubMed]
98. Hatamie, A.; Ren, L.; Dou, H.; Gandasi, N.R.; Rorsman, P.; Ewing, A. Nanoscale Amperometry Reveals That Only a Fraction of Vesicular Serotonin Content Is Released During Exocytosis from Beta Cells. *Angew. Chem. Int. Ed.* **2021**, *60*, 7593–7596. [CrossRef] [PubMed]
99. Wang, N.; Wang, D.; Pan, R.; Wang, D.; Jiang, D.; Chen, H.-Y. Self-Referenced Nanopipette for Electrochemical Analysis of Hydrogen Peroxide in the Nucleus of a Single Living Cell. *Anal. Chem.* **2021**, *93*, 10744–10749. [CrossRef] [PubMed]
100. Ruan, Y.-F.; Wang, H.-Y.; Shi, X.-M.; Xu, Y.-T.; Yu, X.-D.; Zhao, W.-W.; Chen, H.-Y.; Xu, J.-J. Target-Triggered Assembly in a Nanopipette for Electrochemical Single-Cell Analysis. *Anal. Chem.* **2021**, *93*, 1200–1208. [CrossRef] [PubMed]
101. Dick, J.E. Electrochemical Detection of Single Cancer and Healthy Cell Collisions on a Microelectrode. *Chem. Commun.* **2016**, *52*, 10906–10909. [CrossRef] [PubMed]
102. Zhang, F.-L.; Yang, X.-K.; Qi, Y.-T.; Tian, S.-Y.; Huang, W.-H. Nanoelectrochemistry Reveals How Presynaptic Neurons Regulate Vesicle Release to Sustain Synaptic Plasticity under Repetitive Stimuli. *Chem. Sci.* **2024**, *15*, 7651–7658. [CrossRef] [PubMed]
103. Yu, S.-Y.; Zhang, T.-Y.; Liu, Y.-L.; Song, J.; Han, D.-M.; Zhao, W.-W.; Jiang, D.; Xu, J.-J.; Chen, H.-Y. Twin Nanopipettes for Real-Time Electrochemical Monitoring of Cytoplasmic Microviscosity at a Single-Cell Level. *Anal. Chem.* **2021**, *93*, 6831–6838. [CrossRef] [PubMed]
104. Lee, J.; Kang, Y.; Chang, J.; Song, J.; Kim, B.-K. Determination of Serotonin Concentration in Single Human Platelets through Single-Entity Electrochemistry. *ACS Sens.* **2020**, *5*, 1943–1948. [CrossRef] [PubMed]

105. Li, Y.; Zhang, S.; Wang, L.; Xiao, R.; Liu, W.; Zhang, X.; Zhou, Z.; Amatore, C.; Huang, W. Nanoelectrode for Amperometric Monitoring of Individual Vesicular Exocytosis Inside Single Synapses. *Angew. Chem. Int. Ed.* **2014**, *53*, 12456–12460. [CrossRef] [PubMed]
106. Timoshenko, R.V.; Gorelkin, P.V.; Vaneev, A.N.; Krasnovskaya, O.O.; Akasov, R.A.; Garanina, A.S.; Khochenkov, D.A.; Iakimova, T.M.; Klyachko, N.L.; Abakumova, T.O.; et al. Electrochemical Nanopipette Sensor for In Vitro/In Vivo Detection of Cu^{2+} Ions. *Anal. Chem.* **2024**, *96*, 127–136. [CrossRef] [PubMed]
107. Liu, J.; Lu, J.; Ji, W.; Lu, G.; Wang, J.; Ye, T.; Jiang, Y.; Zheng, J.; Yu, P.; Liu, N.; et al. Ion-Selective Micropipette Sensor for In Vivo Monitoring of Sodium Ion with Crown Ether-Encapsulated Metal–Organic Framework Subnanopores. *Anal. Chem.* **2024**, *96*, 2651–2657. [CrossRef] [PubMed]
108. Hao, R.; Zhang, B. Nanopipette-Based Electroplated Nanoelectrodes. *Anal. Chem.* **2016**, *88*, 614–620. [CrossRef] [PubMed]
109. Actis, P.; Tokar, S.; Clausmeyer, J.; Babakinejad, B.; Mikhaleva, S.; Cornut, R.; Takahashi, Y.; López Córdoba, A.; Novak, P.; Shevchuck, A.I.; et al. Electrochemical Nanoprobes for Single-Cell Analysis. *ACS Nano* **2014**, *8*, 875–884. [CrossRef] [PubMed]
110. Pan, R.; Wang, D.; Liu, K.; Chen, H.-Y.; Jiang, D. Electrochemical Molecule Trap-Based Sensing of Low-Abundance Enzymes in One Living Cell. *J. Am. Chem. Soc.* **2022**, *144*, 17558–17566. [CrossRef] [PubMed]
111. Liu, K.; Liu, R.; Wang, D.; Pan, R.; Chen, H.-Y.; Jiang, D. Spatial Analysis of Reactive Oxygen Species in a 3D Cell Model Using a Sensitive Nanocavity Electrode. *Anal. Chem.* **2022**, *94*, 13287–13292. [CrossRef] [PubMed]
112. Gu, H.; Gu, C.; Du Toit, A.; Yu, W.; Chen, M.W.; Struckman, H.L.; Silva, J.R.; Dai, Y.; Ewing, A.G. Single-Entity Resolution Single-Cell Nanosensor Reveals Reactive Oxygen Species at Stress Granules Are Formed by Interfacial Redox Chemistry. *J. Am. Chem. Soc.* **2025**, *147*, 27020–27029. [CrossRef] [PubMed]
113. Ying, Y.-L.; Hu, Y.-X.; Gao, R.; Yu, R.-J.; Gu, Z.; Lee, L.P.; Long, Y.-T. Asymmetric Nanopore Electrode-Based Amplification for Electron Transfer Imaging in Live Cells. *J. Am. Chem. Soc.* **2018**, *140*, 5385–5392. [CrossRef] [PubMed]
114. Roebroek, T.; Van Roy, W.; Roth, S.; Chacon Orellana, L.; Luo, Z.; El Jerrari, Y.; Arnett, C.; Claes, K.; Ha, S.; Jans, K.; et al. Continuous, Label-Free Phenotyping of Single Cells Based on Antibody Interaction Profiling in Microfluidic Channels. *Anal. Chem.* **2025**, *97*, 8975–8983. [CrossRef] [PubMed]
115. Meng, Y.; Wang, S.; Li, J.; Gao, H.; Shang, Y.; Wang, J.; Zhuang, J.; Zhang, D.-W. Label-Free Imaging of Single-Cell Adhesion Using Phase Angle-Responsive Light-Addressable Electrochemical Sensors. *Anal. Chem.* **2025**, *97*, 26211–26218. [CrossRef] [PubMed]
116. Zhang, Y.; Chen, J.; Peng, M.; Meng, X.; Xia, X.-H.; Zhou, Y.-G. Integrated Single-Cell Array-Electrochemical Platform for Label-Free, Nondestructive Longitudinal Tracking of Osteogenic Differentiation. *Anal. Chem.* **2026**, *98*, 8300–8308. [CrossRef] [PubMed]
117. Wang, Q.; Lin, J.; Li, S.; Tian, H.; Zhang, D.; Xin, Q. Label-Free Detection of Single Living Bacteria: Single-Entity Electrochemistry Targeting Metabolic Products. *Anal. Chem.* **2023**, *95*, 13082–13090. [CrossRef] [PubMed]
118. Ronspees, A.T.; Thorgaard, S.N. Blocking Electrochemical Collisions of Single *E. coli* and *B. subtilis* Bacteria at Ultramicroelectrodes Elucidated Using Simultaneous Fluorescence Microscopy. *Electrochim. Acta* **2018**, *278*, 412–420. [CrossRef]
119. Lee, J.Y.; Kim, B.-K.; Kang, M.; Park, J.H. Label-Free Detection of Single Living Bacteria via Electrochemical Collision Event. *Sci. Rep.* **2016**, *6*, 30022. [CrossRef] [PubMed]
120. Gao, G.; Wang, D.; Brocenschi, R.; Zhi, J.; Mirkin, M.V. Toward the Detection and Identification of Single Bacteria by Electrochemical Collision Technique. *Anal. Chem.* **2018**, *90*, 12123–12130. [CrossRef] [PubMed]
121. Zhou, Y.; Dong, J.; Zhao, P.; Zhang, J.; Zheng, M.; Feng, J. Imaging of Single Bacteria with Electrochemiluminescence Microscopy. *J. Am. Chem. Soc.* **2023**, *145*, 8947–8953. [CrossRef] [PubMed]
122. Shkirskiy, V.; Kanoufi, F. Key Requirements for Advancing Machine Learning Approaches in Single Entity Electrochemistry. *Curr. Opin. Electrochem.* **2024**, *46*, 101526. [CrossRef]
123. Vernon, K.L.; Pungsrisai, T.; Wahab, O.J.; Alden, S.E.; Zhong, Y.; Choi, M.-H.; Verma, E.; Bentley, A.K.; Bailey, K.O.; Skrabalak, S.E.; et al. Optically Transparent Carbon Electrodes for Single Entity Electrochemistry. *ACS Electrochem.* **2025**, *1*, 93–102. [CrossRef] [PubMed]
124. Yan, B.; Han, X.; Zhao, R.; Guo, Z.; Li, D.; Yan, Y.; Wang, D.; Yao, X. Simultaneous Electrochemical and SPR Detection of Dopamine Exocytosis from Single Cells and Multiple Cells Using Au Single Atom Modified Carbon Nanopipettes. *Anal. Chem.* **2025**, *97*, 23858–23867. [CrossRef] [PubMed]
125. Zhang, L.; Wahab, O.J.; Jallow, A.A.; O'Dell, Z.J.; Pungsrisai, T.; Sridhar, S.; Vernon, K.L.; Willets, K.A.; Baker, L.A. Recent Developments in Single-Entity Electrochemistry. *Anal. Chem.* **2024**, *96*, 8036–8055. [CrossRef] [PubMed]
126. Clarke, T.B.; Krushinski, L.E.; Vannoy, K.; Colón-Quintana, G.; Roy, K.; Rana, A.; Renault, C.; Hill, M.L.; Dick, J.E. Single Entity Electrocatalysis. *Chem. Rev.* **2024**, *124*, 9015–9080. [CrossRef] [PubMed]

Disclaimer/Publisher's Note: The statements, opinions and data contained in all publications are solely those of the individual author(s) and contributor(s) and not of MDPI and/or the editor(s). MDPI and/or the editor(s) disclaim responsibility for any injury to people or property resulting from any ideas, methods, instructions or products referred to in the content.